HIGHLY EFFICIENT AND EFFECTIVE LLMS WITH MULTI-BOOLEAN ARCHITECTURES

Anonymous authors
Paper under double-blind review

ABSTRACT

Weight binarization has emerged as a promising strategy to reduce the complexity of large language models (LLMs). Existing approaches fall into post-training binarization, which is simple but causes severe performance loss, and training-aware methods, which depend on full-precision latent weights, adding complexity and limiting efficiency. We propose a novel framework that represents LLMs with multi-kernel Boolean parameters and, for the first time, enables direct finetuning LMMs in the Boolean domain, eliminating the need for latent weights. This enhances representational capacity and dramatically reduces complexity during both finetuning and inference. Extensive experiments across diverse LLMs show our method outperforms recent ultra low-bit quantization and binarization techniques.

1 INTRODUCTION

Large language models (Brown et al., 2020; Touvron et al., 2023a; Liu et al., 2024a) have demonstrated unprecedented capabilities, largely due to the continuous growth in both model and dataset sizes. A key area of focus in optimizing these models is lower-precision computation, which offers substantial benefits in terms of memory and computational efficiency. One prominent approach to achieving this is through the quantization of weight parameters, which reduces the model size by lowering the precision of the weight values. Recent studies on scaling laws (Dettmers & Zettlemoyer, 2023; Kumar et al., 2025) have highlighted the potential of using low-precision techniques for large language models (LLMs).

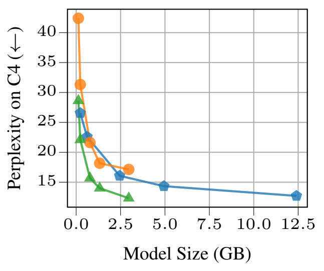

Figure 1: Finetuning OPT models (Zhang et al., 2022) using our 3 Boolean kernels (▲), compared to OPTQ (Frantar et al., 2023) (▲), which quantizes the models to 3 bits, and the FP16 baseline (⬟) on the C4 dataset.

Binarization represents one of the most extreme forms of quantization for LLMs. While significant progress has been made, challenges remain (Yuan et al., 2024; Huang et al., 2024; Li et al., 2025). Even with advanced techniques like Quantization-Aware Training (QAT), which fine-tunes the model extensively after binarization (Xu et al., 2024; Jo et al., 2024), or trains it from scratch (Wang et al., 2023), performance still lags behind that of full-precision (FP) models. This performance gap can be attributed to the limited representation capacity of binary weights and the heavy reliance on FP latent weights for binarization. This reliance not only makes the approach computationally expensive but also suboptimal, as it requires gradient approximation. Meanwhile, recent advances in 4-bit quantization have achieved remarkable compression with minimal accuracy loss, but further compression or applying these methods to smaller models has yielded unsatisfactory results (Frantar et al., 2023; Lin et al., 2024).

In this paper, we aim to push the boundary of low-precision LLMs by proposing a novel method named as Multiple Boolean Kernels (MBOK). We extend the work in Nguyen et al. (2024), which proposes training neural networks with native Boolean weights directly in the Boolean domain, However, effectively applying this approach to LLMs remains a key challenge. In particular, our contributions are:

- We propose the framework MBOK, which employs multiple Boolean kernels, each using distinct Boolean weights (§ 4.2). This allows for flexibly representing LLMs with low bits, while approaching to FP performance with minimal *both* finetuning and inference cost. The Boolean weights are directly trained in Boolean domain, avoiding the need for FP latent weights and gradient approximations.
- We propose a novel successive method that effectively transfers knowledge from an FP LLM into the Boolean model (§ 4.3), followed by further fine-tuning using knowledge distillation (§ 4.3.2).

- We introduce a method for automatically allocating the number of kernels for each weight (§ 5), supporting any average bit-width, including fractional values.
- We provide a comprehensive empirical analysis and benchmarks, demonstrating our method's superior performance over recent binarization and quantization approaches (see § 6) with much lower memory and computational overhead. For example, Fig. 1 shows that our method achieves the best accuracy-compression trade-off, outperforming FP and existing quantization techniques.

2 Related Works

LLMs quantization. Quantization techniques are commonly used to reduce the memory and latency of LLMs. They fall into two categories: QAT, which involves retraining or finetuning in a quantized form, and Post-Training Quantization (PTQ), which can be applied directly without retraining. Due to the difficulty of retraining such large models, most work focuses on PTQ (Frantar et al., 2023; Sheng et al., 2023; Lin et al., 2024; Lee et al., 2024), though recent efforts also explore QAT via data-free methods (LLM-QAT (Liu et al., 2024c)), or parameter-efficient fine-tuning like LoRA (Dettmers et al., 2023). A promient PTQ method is OPTQ (Frantar et al., 2023), which introduces one-shot low-bit weight quantization using approximate second-order information. Follow-up work refines this by addressing outliers (Kim et al., 2024; Dettmers et al., 2024), accounting for activation effects (Lin et al., 2024; Lee et al., 2024), and optimizing quantization parameters (OmniQuant (Shao et al., 2024)). However, effective LLMs quantization is still challenging (Xu et al., 2025).

Binarization. This represents the most extreme form of quantization, typically using the $\mathbf{sign}(\cdot)$ function with gradients estimated via the straight-through-estimator (STE) (Bengio et al., 2013). Early work focused on small Transformer models (Vaswani et al., 2017) trained or fine-tuned on labeled data (Bai et al., 2021; Qin et al., 2022; Liu et al., 2022; 2023). Recent efforts have extended binarization to LLMs. Methods like BiLLM (Huang et al., 2024), PB-LLM (Yuan et al., 2024), STBLLM (Dong et al., 2025), and ARB-LLM (Li et al., 2025) adopt hybrid PTQ approaches, binarizing non-salient weights while using higher precision for important ones, with calibration data used to adjust scaling factors. BitStack (Wang et al., 2025), QBB (Bulat et al., 2024), DB-LLM (Chen et al., 2024) further improve this with multiple binary bases, either through a training-free method or via knowledge distillation. In contrast, BitNet (Wang et al., 2023) replaces linear layers with a custom 1-bit weight structure, BitLinear, and trains the model from scratch. OneBit (Xu et al., 2024), which decomposes weights into 1-bit components and scaling vectors for QAT, further enhanced by MoS (Jo et al., 2024) using a mixture of scalings. Despite progress, these methods remain costly due to their dependence on FP latent weights during training. Table 1 summarizes the key characteristics of these methods in comparison to ours.

Table 1: A summary of SOTA binarization methods for LLMs compared to our method.

Method	Train from Scratch	Post-training Binarization	Finetune from FP Model	Calibration Data	Weight Update	Multiple Binary Bases	Higher-bit Salient Weights
BitNet (Wang et al., 2023)	✓	✗	✗	NA	FP latent-weights	✗	✗
BiLLM (Huang et al., 2024)	✗	✓	✗	✓	NA	✓	✓
PB-LLM (Yuan et al., 2024)	✗	✓	✗	✓	NA	✗	✓
STBLLM (Dong et al., 2025)	✗	✓	✗	✓	NA	✓	✓
ARB-LLM (Li et al., 2025)	✗	✓	✗	✓	NA	✓	✓
BitStack (Wang et al., 2025)	✗	✓	✗	✗	NA	✓	✗
DB-LLM (Chen et al., 2024)	✗	✓	✓	✓	FP latent-weights	✓	✗
QBB (Bulat et al., 2024)	✗	✓	✓	✓	FP latent-weights	✓	✗
OneBit (Xu et al., 2024)	✗	✗	✓	✓	FP latent-weights	✗	✗
MoS (Jo et al., 2024)	✗	✗	✓	✓	FP latent-weights	✗	✗
MBOK [Ours]	✗	✗	✓	✓	Native Boolean weights	✓	✗

3 Preliminaries

Notations. We use a standard notation for vectors ($\mathbf{a}$), matrices ($\mathbf{A}$), and scalars (a). The i-th element of a vector $\mathbf{a}$ is $\mathbf{a}_{[i]}$, and the element at the i-th row and j-th column of a matrix $\mathbf{A}$ is $\mathbf{A}_{[i,j]}$. The symbol $\odot$ denotes element-wise multiplication, with broadcasting if needed.

3.1 Pitfalls of Full-Precision Latent Weights for Binarization

Binarization is an effective technique for reducing both the size and computation of deep learning models by converting high-precision weight parameters into 1-bit values (Hubara et al., 2016; Courbariaux et al., 2015; Rastegari et al., 2016). For a linear layer, $\mathbf{Y} = \mathbf{X}\mathbf{W}_{\text{FP}}^{\top} + \mathbf{b}$, where $\mathbf{X}_{\text{FP}} \in \mathbb{R}^{b \times n}$ is the input data, and $\mathbf{W} \in \mathbb{R}^{m \times n}$ with the input size n and output size m, and $\mathbf{b} \in \mathbb{R}^{m}$

are the FP weights and bias. Binarization results in $\mathbf{Y} = \alpha \cdot \mathbf{X}\mathbf{W}_{\text{bin}}^{\top} + \mathbf{b}$, with $\mathbf{W}_{\text{bin}} = \mathbf{sign}(\mathbf{W}_{\text{FP}})$ and α as a scaling factor (e.g., $\alpha = \frac{\|\mathbf{W}_{\text{FP}}\|_1}{m \times n}$) (Rastegari et al., 2016).

During training, the FP weights must be retained for learning the binarized weights. In vanilla gradient descent, binarized weights are updated as $\mathbf{W}_{\text{bin}} = \mathbf{sign}(\mathbf{W}_{\text{FP}} - \eta \cdot \mathbf{G}_{\mathbf{W}_{\text{FP}}})$, where η is the learning rate and $\mathbf{G}_{\mathbf{W}_{\text{FP}}}$ is the gradient of the FP weights. This leads to high memory usage, especially with optimizers like Adam (Kingma & Ba, 2015), which require storing two additional FP momenta for each parameter. Moreover, the gradient approximation for binarized weights often uses a differentiable proxy, like the STE (Bengio et al., 2013), but this introduces performance drops due to proxy gradient noise. This noise can cause oscillations and instability during training.

3.2 Native Boolean Framework for Neural Networks

To address the issues associated with latent-weight-based approaches, Nguyen et al. (2024) recently proposed a principled framework for directly training Boolean neural networks in the Boolean domain. Consider the l-th Boolean linear layer; in the forward pass, the output of the next layer is defined as:

$$\mathbf{Y}_{[k,j]}^{(l)} = \mathbf{b}_{[j]}^{(l)} + \sum_{i=1}^{n} \mathrm{L}(\mathbf{X}_{[k,i]}^{(l)}, \mathbf{W}_{[i,j]}^{(l)}), \qquad 1 \le j \le m, \tag{1}$$

where k denotes the sample index in the batch, and L is a logic gate such as $\mathbf{and}$, $\mathbf{or}$, $\mathbf{xor}$, or $\mathbf{xnor}$; Hereafter, for clarity, we consider $\mathrm{L} = \mathbf{xnor}$ as a concrete example. The weights $\mathbf{W}_{[i,j]}^{(l)}$ are Boolean values $\{\text{TRUE}, \text{FALSE}\}$ or $\{-1, +1\}$, as typically used in practical implementations.

The logic gate L can be extended to handle mixed-type data. In this paper, we focus on the case where the input data is real-valued, and the weights are Boolean. Specifically, for an input element $x \in \mathbb{R}$, we define $x_{\text{bool}} = \text{TRUE} \Leftrightarrow x \ge 0$, and $x_{\text{bool}} = \text{FALSE} \Leftrightarrow x < 0$, and $|x|$ its magnitude. The logic operation between a real input $x \in \mathbb{R}$ and a Boolean weight $w \in \mathbb{B}$ is defined as $\mathbf{xnor}(w, x) \triangleq s$ such that $s_{\text{bool}} = \mathbf{xnor}(w_{\text{bool}}, x)$ and $|s| = |x|$.

Backward pass. This layer receives the backpropagation signal from the downstream layer. Specifically, $\mathbf{Z}_{[k,j]}^{(l)} \triangleq \frac{\delta \mathcal{L}}{\delta \mathbf{Y}_{[k,j]}^{(l)}}$ denotes the variation of the loss function $\mathcal{L}$ w.r.t. the output at layer l. To optimize the Boolean weights, we need to compute the corresponding loss signal, denoted as $\mathbf{Q}_{[i,j]}^{(l)} \triangleq \frac{\delta \mathcal{L}}{\delta \mathbf{W}_{[i,j]}^{(l)}}$, which is aggregated over the batch dimension k as:

$$\mathbf{Q}_{[i,j]}^{(l)} = \sum_{k=1}^{b} \mathbf{1}(\mathbf{Q}_{[k,i,j]}^{(l)} = \text{TRUE})|\mathbf{Q}_{[k,i,j]}^{(l)}| - \sum_{k=1}^{b} \mathbf{1}(\mathbf{Q}_{[k,i,j]}^{(l)} = \text{FALSE})|\mathbf{Q}_{[k,i,j]}^{(l)}|, \tag{2}$$

where $\mathbf{Q}_{[i,j,k]}^{(l)} = \mathbf{xnor}(\mathbf{Z}_{[k,j]}^{(l)}, \mathbf{X}_{[k,i]}^{(l)})$, and $\mathbf{1}(\cdot)$ is the indicator function. The backpropagation signal for the upstream layer, $\mathbf{P}_{[k,j]}^{(l)} \triangleq \frac{\delta \mathcal{L}}{\delta \mathbf{X}_{[k,j]}^{(l)}}$, can be computed in a similar manner.

Boolean optimizer. Given the loss signal, the rule for updating the Boolean weight $\mathbf{W}_{[i,j]}^{(l)}$ to minimize the loss function $\mathcal{L}$ is as $\mathbf{W}_{[i,j]}^{(l)} = \neg \mathbf{W}_{[i,j]}^{(l)}$ if $\mathbf{xnor}(\mathbf{Q}_{[i,j]}^{(l)}, \mathbf{W}_{[i,j]}^{(l)}) = \text{TRUE}$. Based on this update rule, we can develop an optimizer that accumulates the signal $\mathbf{Q}_{[i,j]}^{(l)}$ over training iterations. Specifically, let $\mathbf{W}_{[i,j]}^{(l),t}$ denotes the weight at iteration t, and $\mathbf{M}_{[i,j]}^{(l),t}$ represents its accumulator, initialized as $\mathbf{M}_{[i,j]}^{(l),0} = 0$. The update rule for the accumulator is then defined as:

$$\mathbf{M}_{[i,j]}^{(l),t+1} \leftarrow \beta^t \mathbf{M}_{[i,j]}^{(l),t} + \eta \mathbf{Q}_{[i,j]}^{(l),t}, \tag{3}$$

where η is the accumulation factor acting as a learning rate, and β^t is a regularizing factor that reflects the system's state at time t. In our work, we use brain plasticity (Fuchs et al., 2014) and Hebbian theory (Hebb, 2005) to adaptively set β^t. We encourage the reader check Appendix A for details.

Remarks on complexity and applicability to LLMs. This Boolean framework optimizes Boolean parameters $\mathbf{W}_{[i,j]}^{(l)}$ directly in the Boolean space, eliminating the need for FP latent weights. As shown in Eq. 3, the Boolean optimizer is more lightweight than common LLM optimizers like Adam, requiring only one FP momentum per parameter. This reduces both training and inference complexity and avoids gradient approximation induced from STE. As shown in Proposition A.10 in Appendix, $\mathbf{xnor}(w, s) = w \times s$, mathematically enabling direct application to existing linear algebra operations. Practically, native logic operations are much faster than multiplication.

4 Multiple Boolean Kernels

4.1 Boolean Reformulation for Linear Layers

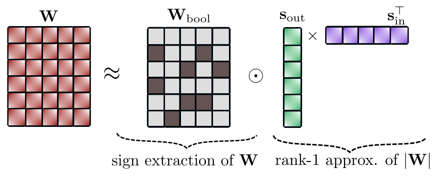
$\mathbf{W}$
$\approx$
$\mathbf{W}_{\text{bool}}$
$\odot$
$\mathbf{s}_{\text{out}}$
$\times$
$\mathbf{s}_{\text{in}}^{\top}$
sign extraction of $\mathbf{W}$
rank-1 approx. of $|\mathbf{W}|$

Figure 2: Illustration of SVID.

LLMs (Brown et al., 2020) are mostly based on the Transformer architecture (Vaswani et al., 2017), in which linear layers are the core elements. Inpsired by Xu et al. (2024), we employ sign-value-independent decomposition (SVID) such that an FP input matrix $\mathbf{W} \in \mathbb{R}^{m\times n}$ of linear layers is decomposed into one Boolean matrix $\mathbf{W}_{\text{bool}} \triangleq \mathbf{sign}(\mathbf{W})$ and two FP vectors $\mathbf{s}_{\text{in}}$ and $\mathbf{s}_{\text{out}}$. Precisely, let $|\mathbf{W}|$ be the element-wise absolute value of $\mathbf{W}$, write $|\mathbf{W}| = \mathbf{U}\mathbf{\Sigma}\mathbf{V}^{\top}$ its singular value decomposition (SVD) (Beltrami, 1990). Using rank-1 approximation of $|\mathbf{W}|$, $\mathbf{s}_{\text{in}}$ and $\mathbf{s}_{\text{out}}$ are given as: $\mathbf{s}_{\text{in}} = \sqrt{\sigma_1}\mathbf{V}_{[:,1]}$, and $\mathbf{s}_{\text{out}} = \sqrt{\sigma_1}\mathbf{U}_{[:,1]}$. Then, the input matrix is approximated as $\mathbf{W} = \mathbf{W}_{\text{bool}} \odot |\mathbf{W}| \approx \mathbf{W}_{\text{bool}} \odot \left(\mathbf{s}_{\text{out}}\mathbf{s}_{\text{in}}^{\top}\right)$. This procedure is illustrated in Fig. 2.

Proposition 4.1. *(Xu et al., 2024) For $\mathbf{W} \in \mathbb{R}^{m\times n}$, write $\mathbf{W} = \widetilde{\mathbf{U}}\widetilde{\mathbf{\Sigma}}\widetilde{\mathbf{V}}^{\top}$ its SVD. Let $\mathbf{a} = \sqrt{\widetilde{\sigma}_1}\widetilde{\mathbf{U}}_{[:,1]}$, and $\mathbf{b} = \sqrt{\widetilde{\sigma}_1}\widetilde{\mathbf{V}}_{[:,1]}$. With the notations as described above, we have:*

$$\left\|\mathbf{W} - \mathbf{W}_{\text{bool}} \odot \mathbf{s}_{\text{out}}\mathbf{s}_{\text{in}}^{\top}\right\|_F^2 \le \left\|\mathbf{W} - \mathbf{a}\mathbf{b}^{\top}\right\|_F^2. \tag{4}$$

Remark 4.2. Proposition 4.1 re-states Proposition 2 of Xu et al. (2024) with its precise assumption of vectors $\mathbf{a}$ and $\mathbf{b}$ which is necessary for its proof provided in Appendix therein.

Proposition 4.1 shows that using $\mathbf{W}_{\text{bool}}$ together with value matrix approximation is better than a direct rank-1 approximation of $\mathbf{W}$ in terms of Frobenius-norm. This emphasizes the important role of $\mathbf{W}_{\text{bool}}$ in approximating the original FP matrix. Moreover, our following Proposition 4.3 shows that the SVID approximation as described above is optimal for approximating the original matrix $\mathbf{W}_{\text{bool}}$.

Proposition 4.3. *For $\mathbf{W} \in \mathbb{R}^{m\times n}$ and the notations as described above, we have:*

$$\left\|\mathbf{W} - \mathbf{W}_{\text{bool}} \odot \mathbf{s}_{\text{out}}\mathbf{s}_{\text{in}}^{\top}\right\|_F^2 \le \left\|\mathbf{W} - \mathbf{W}_{\text{bool}} \odot \mathbf{c}\mathbf{d}^{\top}\right\|_F^2, \quad \forall \mathbf{c} \in \mathbb{R}^{m\times 1}, \forall \mathbf{d} \in \mathbb{R}^{n\times 1}. \tag{5}$$

The proof is given in Appendix D.3. The linear layer can be then reformulated as (Xu et al., 2024):

$$\mathbf{X}\mathbf{W}_{\text{FP}}^{\top} \approx \left[\left(\mathbf{X} \odot \mathbf{s}_{\text{in}}^{\top}\right)\mathbf{W}_{\text{bool}}\right] \odot \mathbf{s}_{\text{out}}^{\top}. \tag{6}$$

4.2 Enhanced Expressivity with Multiple Boolean Kernels

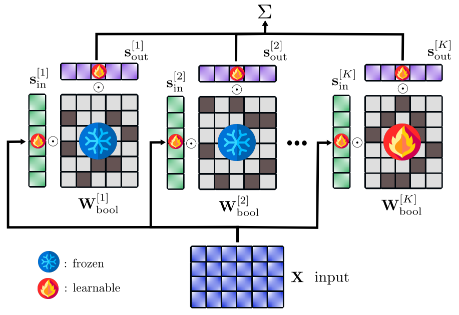
Σ
$\mathbf{s}_{\text{out}}^{[1]}$
$\mathbf{s}_{\text{out}}^{[2]}$
$\mathbf{s}_{\text{out}}^{[K]}$
$\mathbf{s}_{\text{in}}^{[1]}$
$\mathbf{s}_{\text{in}}^{[2]}$
$\mathbf{s}_{\text{in}}^{[K]}$
$\odot$
$\mathbf{W}_{\text{bool}}^{[1]}$
$\mathbf{W}_{\text{bool}}^{[2]}$
$\mathbf{W}_{\text{bool}}^{[K]}$
: frozen
: learnable
$\mathbf{X}$ input

Figure 3: The computation of a linear layer approximated using multi kernels of Boolean.

We have shown that SVID provides a good approximation of the original weights, its expressivity can be still limited to capture well the original FP parameters of complicated models, which were trained on large-scale datasets over extended periods of time. To overcome this limitation, we propose the use of a multi-Boolean kernel structure for the weights. Specifically, we employ K kernels, where each kernel utilizes distinct Boolean weights and scaling factors, to better represent the original weight parameters. This leads to the approximation: $\mathbf{W}_{\text{FP}} \approx \mathbf{W}_{\text{approx}} \triangleq \sum_{k=1}^{K} \mathbf{W}_{\text{bool}}^{[k]} \odot (\mathbf{s}_{\text{out}}^{[k]}\mathbf{s}_{\text{in}}^{[k]\top})$. The computation of a linear layer can then be approximated as follows (see Fig. 3 for an illustration):

$$\mathbf{X}\mathbf{W}_{\text{FP}}^{\top} \approx \sum_{k=1}^{K}\left[\left(\mathbf{X} \odot \mathbf{s}_{\text{in}}^{[k]\top}\right)\mathbf{W}_{\text{bool}}^{[k]}\right] \odot \mathbf{s}_{\text{out}}^{[k]\top}. \tag{7}$$

Here, the computational costs associated with the FP scaling factors, $\mathbf{s}_{\text{in}}$ and $\mathbf{s}_{\text{out}}$, are small because they only involve element-wise multiplications. The dominant computational cost arises from the matrix multiplication between the scaled input data, $\mathbf{X} \odot \mathbf{s}_{\text{in}}$, and the weights. However, thanks to the use of Boolean weights, the complexity is significantly reduced, as these multiplications can be replaced by additions. Moreover, as we will demonstrate in § 6.1.1, only a small number of kernels are required to achieve a reasonable result. Additionally, we find that, after the successive extraction process from the FP model (§ 4.3.1), we only need to train the Boolean weights for the last kernel and the scaling factors, further significantly reducing the overall complexity.

4.3 Effective Knowledge Transfer into Boolean Models

We have introduced our proposed multi-Boolean kernel structure for effectively representing the linear layers of LLMs. In this section, we outline the process for transferring knowledge from a source FP model to a Boolean model. This process consists of two steps: (1) data-free initialization to maximize information retention from the source, and (2) data-dependent finetuning, where the Boolean model is further trained on a target dataset with guidance from the FP model.

4.3.1 Successive Extraction using SVID

For each linear layer, to initialize the values of the Boolean weights and scaling factors for all kernels, we successively apply SVID to the given FP weights. The goal here is to further proceed to SVID process to approximate the residual error introduced by the previous step. Specifically, after each step of decomposing the weight matrix using SVID, we obtain a residual matrix, which is defined as:

$$\mathbf{W}_{\text{res}}^{[k]} = \mathbf{W}_{\text{input}}^{[k]} - \mathbf{W}_{\text{bool}}^{[k]} \odot \left(\mathbf{s}_{\text{out}}^{[k]} \mathbf{s}_{\text{in}}^{[k]\top} \right). \tag{8}$$

Here, $\mathbf{W}_{\text{res}}^{[k]}$ is the residual matrix, and $\mathbf{W}_{\text{bool}}^{[k]}$, $\mathbf{s}_{\text{out}}^{[k]}$ and $\mathbf{s}_{\text{in}}^{[k]}$ are the extracted parameters for the k-th kernel, while $\mathbf{W}_{\text{input}}^{[k]}$ represents the input FP matrix for step k. For the first step, this is the original weight matrix, and for subsequent steps, it is the residual matrix obtained from the previous step.

Fig. 4 illustrate this process. Although using multiple kernels effectively captures the original weight matrix, a residual error still remains at the end of the process. While this residual error is small, it can accumulate as it propagates through the layers, finally leading to predictions that diverge from those of the original FP model. To address this issue, it is necessary to further finetune the resulting model to compensate for these errors and make it better suited to the target task. We will discuss this in § 6.1.2. In the following section, we will introduce knowledge distillation to achieve this goal.

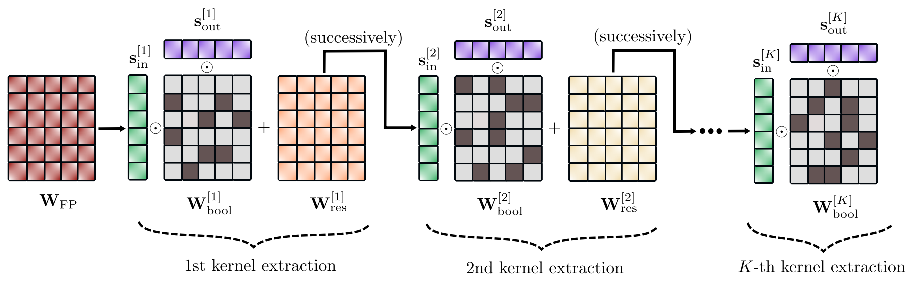
$\mathbf{s}_{\text{out}}^{[1]}$
$\mathbf{s}_{\text{in}}^{[1]}$
(successively)
$\mathbf{s}_{\text{out}}^{[2]}$
$\mathbf{s}_{\text{in}}^{[2]}$
(successively)
$\mathbf{s}_{\text{out}}^{[K]}$
$\mathbf{s}_{\text{in}}^{[K]}$
$\mathbf{W}_{\text{FP}}$
$\mathbf{W}_{\text{bool}}^{[1]}$
$\mathbf{W}_{\text{res}}^{[1]}$
$\mathbf{W}_{\text{bool}}^{[2]}$
$\mathbf{W}_{\text{res}}^{[2]}$
$\mathbf{W}_{\text{bool}}^{[K]}$
1st kernel extraction
2nd kernel extraction
K-th kernel extraction

Figure 4: Illustration of successive extractions of Boolean kernels from a given FP weight matrix.

4.3.2 Finetuning with Knowledge Distillation

Knowledge distillation (KD) (Hinton et al., 2015) trains a student network to mimic a more powerful teacher, usually with greater efficiency. The student learns from the teacher's output distribution and/or intermediate states as "soft targets". Here, the FP model is the teacher and the Boolean model the student. Specifically, the output probability distribution of an LLM for a token $\mathbf{X}_{[i]}$ is:

$$p(\mathbf{X}_{[i]};\tau) = \frac{\exp(\mathbf{X}_{[i]}/\tau)}{\sum_{j=1}^{N_V} \exp(\mathbf{X}_{[j]}/\tau)}, \tag{9}$$

where N_V is the vocabulary size and τ is the softmax temperature. The logit-based knowledge distillation (KD) loss across the sequence of all output tokens is defined as follows:

$$\mathcal{L}_{\text{logits}} = \frac{1}{L} \sum_{j=1}^{L} \text{D}_{\text{logits}} \left(p_{\text{FP}}(\mathbf{X}_{[j]};\tau), p_{\text{bool}}(\mathbf{X}_{[j]};\tau) \right). \tag{10}$$

Here, $p_{\text{FP}}(\mathbf{X}_{[j]};\tau)$ and $p_{\text{bool}}(\mathbf{X}_{[j]};\tau)$ denote the distributions over the j-th token from the FP and Boolean models, respectively, with L as the sequence length. We find that $\tau = 1$ works best in practice. Among possible measures for D_{logits} (Ko et al., 2024), the forward Kullback–Leibler (KL) divergence gives the strongest results; further discussion is in Appendix G.2.

To further reduce distributional discrepancies in intermediate layers, we additionally employ an intermediate state–based KD loss over a sequence of hidden states:

$$\mathcal{L}_{\text{is}} = \frac{1}{L} \sum_{h \in H} \sum_{j=1}^{L} \left\| \mathbf{Q}_{\text{FP}}^{j,h} - \mathbf{Q}_{\text{bool}}^{j,h} \right\|_2^2, \tag{11}$$

where $\mathbf{Q}_{\text{FP}}^{j,h}$ and $\mathbf{Q}_{\text{bool}}^{j,h}$ represent the h-th hidden states of the FP and Boolean models for the j-th token, repsectively; H is the set of chosen intermediate states. Finally, the overall loss is then computed as $\mathcal{L} = \mathcal{L}_{\text{logits}} + \gamma \mathcal{L}_{\text{is}}$, where γ is a weighted factor that balances the contribution of the two losses. We empirically found that $\gamma = 10$ works best.

5 Kernel Allocation

Using more kernels enhances the Boolean model's representational capacity but also increases its size. We propose a method to automatically allocate kernels per weight under a fixed budget. Let $N_{\mathbf{W}}$ be the number of weights in the FP teacher model, and K_l for $l \in [1, N_{\mathbf{W}}]$ the number of Boolean kernels for the l-th weight. Our goal is to determine $\mathbf{k} \triangleq \{K_l\}_{l \in [1, N_{\mathbf{W}}]}$ subject to design constraints. Key factors include:

(1) Residual error: Let $e_l^{[k]} \in \mathbb{R}$ denote the approximation error from applying the successive SVID extraction to the k-th kernel of the l-th weight, measured by the Frobenius norm of $\mathbf{W}_{\text{res}}^{[k]}$ (Eq. 8).

(2) Weight importance: Let h_l denote the importance of the l-th weight in the FP teacher model. Higher scores indicate the need for more Boolean kernels. We propose estimating h_l using projection weighted canonical correlation analysis (PWCCA) (Morcos et al., 2018), a reliable method for analyzing deep model representations. Details are provided in Appendix E.1.

(3) Weight size: The size of the l-th weight is denoted by s_l and $p_l \triangleq s_l / \sum_{k=1}^{N_{\mathbf{W}}} s_k$ represents its relative size in the model.

For a given $\mathbf{k}$, the size of the target Boolean model, in terms of the number of weights, is $\sum_{l=1}^{N_{\mathbf{W}}} K_l s_l$. Relative to the source FP model, this repersents an expansion ratio, defined as:

$$\rho(\mathbf{k}) \triangleq \frac{\sum_{l=1}^{N_{\mathbf{W}}} K_l s_l}{\sum_{l=1}^{N_{\mathbf{W}}} s_l} = \sum_{l=1}^{N_{\mathbf{W}}} K_l p_l. \tag{12}$$

Optimization objective. To control model size, we constrain the expansion ratio to a target $T \geq 1$ and limit the kernel size by $K_{\max}$, with $T \leq K_{\max} \leq \infty$. The optimization space is thus $\mathcal{K} \triangleq [1, K_{\max}]^{N_{\mathbf{W}}}$, and the problem is formulated as:

$$\mathbf{k}^* = \arg\min_{\mathbf{k} \in \mathcal{K}} \mathcal{E}(\mathbf{k}), \quad \text{s.t.} \quad \rho(\mathbf{k}) \leq T, \quad \text{where } \mathcal{E}(\mathbf{k}) \triangleq \sum_{l=1}^{N_{\mathbf{W}}} h_l e_l^{[K_l]} f(p_l). \tag{13}$$

Here, $\mathcal{E}(\mathbf{k})$ is the objective (energy) function, and $f(\cdot)$ is a monotonically decreasing function. In practice, we use $f(p_l) = (1/p_l) \log(1/p_l)$. Intuitively, the goal is to minimize residual error while prioritizing weights with higher importance and smaller size, balancing accurate knowledge transfer with model efficiency.

Optimization algorithm. The problem has complexity $\mathcal{O}(K_{\max}^{N_{\mathbf{W}}})$, which is prohibitive for LLMs. To tackle this NP-hard problem efficiently, we note that $e_l^{[k]}$ decreases with k for all l, and $\mathcal{E}(\mathbf{k})$ is maximized at $\mathbf{k} = \mathbf{1}$, with any increase in k_l reducing $\mathcal{E}(\mathbf{k})$. This motivates a heuristic iterative approach: at each step, increment the K_l that yields the largest reduction in $\mathcal{E}(\mathbf{k})$. The full algorithm is given in Algorithm 9 in the Appendix. We will demonstrate in § 6.5 the practicality of our method.

6 Experiments

Setups. In all experiments, we follow the protocol from Jo et al. (2024), without quantizing activations. The training set combines WikiText2 (Merity et al., 2017) and a selected partition of C4 (Raffel et al., 2020) data, using sequences of length 2048. We apply a cosine decay learning rate with a 3% warm-up over 3 epochs and batch size 8. Boolean parameters use a maximum learning rate of 5×10^{-3}, while remaining FP parameters are optimized with AdamW (Loshchilov & Hutter, 2019) at a maximum learning rate of 2×10^{-5}, with $\beta_1 = 0.9$ and $\beta_2 = 0.999$. Following standard practice (Jo et al., 2024), performance is evaluated via perplexity on WikiText2 and C4 (lower is better).

6.1 Ablation Studies and Analysis

6.1.1 Effect of the number of kernels

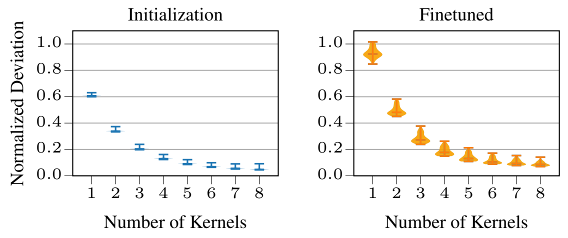

Perplexity (↓)

#Kernels	1	2	3	4
Wiki2	39.38	31.47	29.10	28.52
C4	35.44	28.62	26.48	25.90
#Kernels	**5**	**6**	**7**	**8**
Wiki2	28.19	28.16	28.13	28.08
C4	25.65	25.50	25.40	25.31

Figure 5: Normalized L1 norm difference between the approximated weights at initialization and after finetuning against the FP weights ($\|\mathbf{W}_{\text{approx}} - \mathbf{W}_{\text{FP}}\|_1 / \|\mathbf{W}_{\text{FP}}\|_1$) , and the final results.

We begin by examining the effect of the number of Boolean kernels on OPT-125M model (Zhang et al., 2022). Fig. 5 shows the normalized difference between weights approximated via successive SVID and the original FP weights, both at initialization and after finetuning. Increasing the number of kernels reduces approximation error and improves perplexity, unlike MoS (Jo et al., 2024), where adding more experts does not always help and can even hurt performance. Using 3–4 kernels yields a good approximation, with diminishing improvements beyond that. Interestingly, the normalized difference relative to the full FP weights is larger after KD finetuning. We hypothesize that KD compensates the errors due to the lower expressiveness of a small number of kernels, further emphasizing its role in adapting the model to approximate the FP model rather than exactly replicating each weight.

6.1.2 Optimization strategy

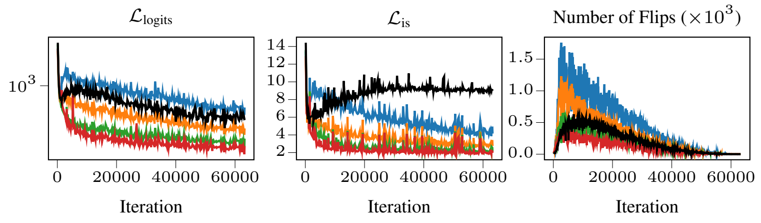

Optim. Kernel	Wiki2	C4
🟦 1st	33.90	30.70
🟧 2nd	30.29	27.55
🟩 3rd	29.00	26.36
🟥 4th	**28.60**	**25.93**
⬛ All	32.04	29.08

Figure 6: The progression of training losses, number of flips, and perplexity of the resulting models (OPT-125M) is examined with respect to the optimization of different kernel configurations.

Next, we study the effect of optimizing kernels on the OPT-125M model. We consider four Boolean kernels but train only one at a time, keeping the others frozen. Fig. 6 shows the loss convergence. Training the first kernel converges slowest, while higher-order kernels improve progressively. As shown in Proposition 4.1 and Proposition 4.3, the SVID effectively extracts optimal Boolean weights and scaling factors. In our successive SVID framework, the first kernel is well extracted and captures the most important information, and higher-order kernels approximate residuals. Since the kernels are related in a successive manner, modifying lower-order kernels affects higher-order ones. We observe that training only the first kernel results in many weight flips, indicating optimization difficulty, whereas fine-tuning only the last kernel efficiently compensates for residual errors, showing the lowest flip rates and best performance. This is in line with the observation by Liu et al. (2024b), where they compress "delta" induced by the finetuning process by using 1-bit weights. This further highlights the advantage of our approach, as training complexity is significantly reduced by only optimizing the last kernel. Thus, we apply this strategy in all our experiments.

6.2 Main Benchmark Results

Table 2 compares our method with recent baselines in binarization and 2-bit quantization, evaluating perplexity and accuracy on zero-shot tasks including Winogrande (Sakaguchi et al., 2021), HellaSwag (Zellers et al., 2019), PIQA (Bisk et al., 2020), BoolQ (Clark et al., 2019), and ARC (Clark et al., 2018). For our method, we use 2 Boolean kernels, an ultra low-bit setting. Due to space constraints, the results for LLaMA2-7B and LLaMA2-13B (Touvron et al., 2023b) and different number of Boolean kernels are provided in Appendix G.4 and Appendix G.3. We note that our method is close to scalar quantization while being completely orthogonal to vector quantization (VQ) which adds substantial overhead (Gray, 1984). For completeness, we encourage the reader refer to Appendix G.11 for VQ comparisons, and Appendix G.6 for further baselines.

Our method consistently and significantly outperforms the baselines in both perplexity and zero-shot accuracy, achieving results close to the FP16 baseline despite using only a budget of 2 bits for weight. As expected, QAT methods like OneBit and MoS perform better than PTQ methods, but this comes at the cost of extensive finetuning. In contrast, our approach efficiently address this problem by optimizing parameters directly in Boolean space, avoiding the need for optimizing in FP latent sapce.

Table 2: Perplexity and zero-shot accuracy results of Float16, quantized and binarized LLMs.

Model	Method	Wbits	Perplexity (↓)		Zero-shot Accuracy (↑)						
			Wiki2	C4	BoolQ	PIQA	Hella.	WinoG.	ARC-e	ARC-c	Average
OPT-1.3B	FP16	16	14.62	14.72	57.82	72.42	53.70	59.51	50.97	29.52	53.99
	PB-LLM	1.7	272.83	175.42	62.17	54.24	27.25	50.27	27.98	23.72	40.94
	BiLLM	1.11	69.45	63.92	61.92	59.52	33.81	49.32	34.38	22.35	43.55
	OneBit	1	20.36	20.76	57.85	66.53	39.21	54.61	42.80	23.97	47.50
	MoS	1	18.45	18.83	60.34	68.66	41.99	53.99	44.87	26.19	49.34
	OPTQ	2	9.5e3	3.8e3	39.60	52.07	25.57	49.33	26.68	23.63	35.15
	LLM-QAT	2	4.9e3	2.1e3	37.83	50.05	25.72	49.72	25.76	25.09	34.07
	OmniQuant	2	42.43	55.64	56.45	60.94	33.39	51.85	38.76	23.38	44.13
	MBOK [Ours]	2×1	**16.13**	**16.61**	58.53	70.67	48.11	56.75	48.19	27.90	**51.69**
LLaMA-7B	FP16	16	5.68	7.08	73.21	77.42	72.99	66.85	52.53	41.38	64.06
	PB-LLM	1.7	198.37	157.35	60.51	53.53	27.23	49.17	27.48	26.02	40.66
	BiLLM	1.11	41.66	48.15	62.23	58.65	34.64	51.14	33.08	25.68	44.24
	OneBit	1	8.48	10.49	62.50	70.40	54.03	55.32	41.07	30.88	52.36
	MoS	1	7.97	9.72	64.59	71.82	58.18	58.88	42.09	31.31	54.48
	OPTQ	2	1.9e3	7.8e2	43.79	49.95	25.63	49.41	25.84	27.47	37.02
	LLM-QAT	2	7.1e2	3.0e2	37.83	50.87	24.76	51.78	26.26	25.51	36.17
	OmniQuant	2	15.34	26.21	58.69	62.79	43.68	52.96	41.54	29.35	48.17
	MBOK [Ours]	2×1	**6.83**	**8.53**	69.20	74.32	64.80	60.30	49.05	34.90	**58.76**
LLaMA-13B	FP16	16	5.09	6.61	68.47	79.05	76.24	70.17	59.85	44.54	66.39
	PB-LLM	1.7	35.83	39.79	62.17	58.70	33.97	52.17	31.86	23.63	43.75
	BiLLM	1.11	14.56	16.67	62.53	68.17	52.24	59.43	41.91	29.94	52.37
	OneBit	1	7.65	9.56	63.30	71.98	60.61	59.43	42.85	32.42	55.10
	MoS	1	7.16	8.81	63.82	73.88	64.05	60.93	44.28	33.11	56.68
	OPTQ	2	3.2e3	9.9e2	42.39	50.00	25.27	50.67	26.14	27.39	36.98
	LLM-QAT	2	1.8e3	1.2e3	37.83	50.33	25.40	51.62	27.02	26.87	36.51
	OmniQuant	2	13.43	19.33	62.20	68.99	54.16	53.83	45.50	30.38	52.51
	MBOK [Ours]	2×1	**6.17**	**7.88**	68.10	76.33	69.88	64.17	52.34	37.88	**61.45**

6.3 Accuracy-Compression Trade-offs

We further investigate the accuracy-compression trade-offs of our method, quantization methods, and the FP model. Specifically, we compare 3-bit quantization using round-to-nearest (RTN) (Yao et al., 2022; Dettmers et al., 2022) and OPTQ (Frantar et al., 2023) methods against our approach using 3 Boolean kernels. We evaluate these methods on OPT models of varying sizes. The results, presented in Table 3 and Fig. 1, show that with 3 kernels, our method closely approaches the performance of the FP model. Given the same weight budget, our method clearly sits on the Pareto frontier, delivering the best performance for the same model size.

Table 3: OPT perplexity results (*lower is better*) on WikiText2 and C4. The results of FP, rount-to-nearest (RTN) and OPTQ are taken from (Frantar et al., 2023).

OPT Model	WBits	Wiki2					C4				
		125M	350M	1.3B	2.7B	6.7B	125M	350M	1.3B	2.7B	6.7B
FULL-PRECISION	16	27.65	22.00	14.63	12.47	10.86	26.56	22.59	16.07	14.34	12.71
RTN (Yao et al., 2022; Dettmers et al., 2022)	3	1.3e3	64.57	1.3e4	1.6e4	5.8e3	834	55.49	5.2e3	1.1e4	5.3e3
OPTQ (Frantar et al., 2023)	3	53.85	33.79	20.97	16.88	14.86	42.41	31.33	21.63	18.17	17.14
MBOK [Ours]	3×1	**29.10**	**23.12**	**15.30**	**13.09**	**11.03**	**28.62**	**22.10**	**15.68**	**14.00**	**12.33**

6.4 Comparison with Latent-weight Approaches

We compare our method with latent-weight approaches on OPT models, using MoS with 3 experts and our method with 3 Boolean kernels. We also introduce a baseline using our SVID framework to construct 3 binary weights that rely on FP latent weights for training. Results in Fig. 7 show that our method converges much faster, as it directly optimizes Boolean parameters without the need for STE to approximate gradient signals. Both our approach and the latent-weight method outperform MoS, demonstrating the benefit of using additional Boolean kernels and our successive SVID framework. Our method is also more efficient, avoiding the need for FP latent weights and extra momentum.

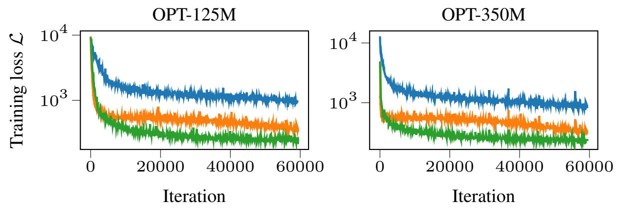

OPT	Method	Wiki2	C4
125M	MoS (3 experts)	38.62	34.72
	3 Latent weights	29.47	27.18
	MBOK (3 kernels) [Ours]	**29.10**	**26.48**
350M	MoS (3 experts)	29.93	28.25
	3 Latent weights	23.58	22.65
	MBOK (3 kernels) [Ours]	**23.12**	**22.10**

Figure 7: Comparions between our method and latent-weight approaches.

6.5 Kernel Allocation and Comparison to BitNet b1.58

We next evaluate our kernel allocation method on the OPT-125M model. It supports bit allocation at any granularity, including fractional averages, providing practitioners with a flexible model selection tool under deployment constraints. Fig. 10 reports results for varying average bit budgets, showing consistent improvements as the budget increases. Fig. 9 illustrates kernel allocation with a 3.5-bit average, where more kernels are assigned to FC2 and output projection layers in the final blocks. This aligns with prior observations (Bondarenko et al., 2023; Frantar et al., 2023) that these layers are particularly important and sensitive to compression.

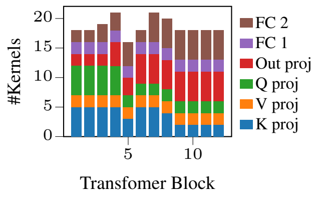

Figure 9: Allocated kernels for OPT-125M.

In addition, our framework's flexibility enables direct comparison with BitNet-b1.58 (Ma et al., 2024), which employs ternary weights. With a 1.58-bit budget, our model achieves reasonable results, whereas BitNet-b1.58 reaches a C4 perplexity of 10199.89 due to finetuning instability, consistent with Xu et al. (2024). We also compare against ShiftAddLLM (You et al., 2024), a PTQ method supporting bit allocation. Our approach performs substantially better (32.23 with a 2-bit budget vs. 435.84 for their mixed 2.2-bit allocation, see Table 17 in ShiftAddLLM).

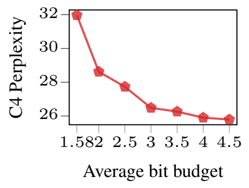

Figure 10: OPT-125M performance w.r.t. bit budget.

6.6 Discussion on Complexity

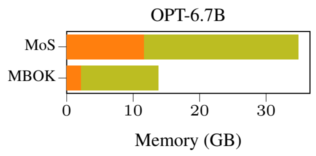

Figure 11: Estimated memory for finetuning for weights (🟧) and optimizer states (🟩).

We emphasize the efficiency of our method during finetuning by comparing MoS (Jo et al., 2024) with our approach using 3 Boolean kernels on the OPT-6.7B model. Because we optimize directly in the Boolean domain, each weight requires only 1 bit, whereas MoS relies on 16-bit latent weights. Moreover, we finetune only the last Boolean kernel, with the optimizer storing a single 16-bit momentum per weight. In contrast, Adam (Kingma & Ba, 2015) for latent weights needs two 16-bit momenta per weight. Fig. 11 shows the estimated memory for a minibatch of one, highlighting the substantial memory savings of our method. These gains could be further amplified by incorporating optimizer state compression techniques such as GaLore (Zhao et al., 2024). We also provide a theoretical analysis of finetuning complexity in Appendix F, and empirical evidence (Appendix G.11) demonstrating significant GPU latency gains: using BitBlas library (Wang et al., 2024), our method achieves up to over 8.7× speedup for LLaMA2 layers compared to FP16, with even more improvements expected on native Boolean accelerators.

7 Conclusions

We introduced Multiple Boolean Kernels (MBOK), a novel framework for low-bit finetuning LLMs. By utilizing Boolean weights and optimizing them directly in the Boolean domain, our framework significantly reduces both memory and computation costs during *both* finetuning and inference. The flexible multi-Boolean structure, along with the proposed successive SVID, effectively transfers knowledge from a source FP model. Through extensive experiments on LLMs of various sizes, we demonstrate that our method approaches FP performance while achieving the best accuracy-compression trade-off compared to existing quantization and binarization methods.

Limitations. Our method, like other binarized neural networks, could not be assessed on native Boolean accelerators due to hardware being optimized for real arithmetic. Nevertheless, we demonstrated strong results even on modern hardware, underscoring the promise of our approach and motivating future development of accelerators tailored to Boolean computation.

REFERENCES

Rishabh Agarwal, Nino Vieillard, Yongchao Zhou, Piotr Stanczyk, Sabela Ramos Garea, Matthieu Geist, and Olivier Bachem. On-Policy Distillation of Language Models: Learning from Self-Generated Mistakes. In *The Twelfth International Conference on Learning Representations*, 2024. URL https://openreview.net/forum?id=3zKtaqxLhW.

Haoli Bai, Wei Zhang, Lu Hou, Lifeng Shang, Jin Jin, Xin Jiang, Qun Liu, Michael Lyu, and Irwin King. BinaryBERT: Pushing the Limit of BERT Quantization. In *Proceedings of the 59th Annual Meeting of the Association for Computational Linguistics and the 11th International Joint Conference on Natural Language Processing (Volume 1: Long Papers)*, pp. 4334–4348, Online, 2021. Association for Computational Linguistics. URL https://aclanthology.org/2021.acl-long.334/.

E Beltrami. Sulle funzioni bilineari, giomale di mathematiche ad uso studenti delle uninersita. 11, 98–106.(an english translation by d boley is available as university of minnesota, department of computer science). Technical report, Technical Report 90–37, 1990.

Yoshua Bengio, Nicholas Léonard, and Aaron Courville. Estimating or Propagating Gradients Through Stochastic Neurons for Conditional Computation. *arXiv preprint arXiv:1308.3432*, 2013.

Yonatan Bisk, Rowan Zellers, Jianfeng Gao, Yejin Choi, et al. PIQA: Reasoning about Physical Commonsense in Natural Language. In *Proceedings of the AAAI conference on artificial intelligence*, volume 34, pp. 7432–7439, 2020.

Yelysei Bondarenko, Markus Nagel, and Tijmen Blankevoort. Quantizable Transformers: Removing Outliers by Helping Attention Heads Do Nothing. In *Advances in Neural Information Processing Systems*, volume 36, pp. 75067–75096. Curran Associates, Inc., 2023. URL https://proceedings.neurips.cc/paper_files/paper/2023/file/edbcb7583fd8921dad78adecfe06a99b-Paper-Conference.pdf.

Tom Brown, Benjamin Mann, Nick Ryder, Melanie Subbiah, Jared D Kaplan, Prafulla Dhariwal, Arvind Neelakantan, Pranav Shyam, Girish Sastry, Amanda Askell, Sandhini Agarwal, Ariel Herbert-Voss, Gretchen Krueger, Tom Henighan, Rewon Child, Aditya Ramesh, Daniel Ziegler, Jeffrey Wu, Clemens Winter, Chris Hesse, Mark Chen, Eric Sigler, Mateusz Litwin, Scott Gray, Benjamin Chess, Jack Clark, Christopher Berner, Sam McCandlish, Alec Radford, Ilya Sutskever, and Dario Amodei. Language Models are Few-Shot Learners. In *Advances in Neural Information Processing Systems*, volume 33, pp. 1877–1901. Curran Associates, Inc., 2020. URL https://proceedings.neurips.cc/paper_files/paper/2020/file/1457c0d6bfcb4967418bfb8ac142f64a-Paper.pdf.

Adrian Bulat, Yassine Ouali, and Georgios Tzimiropoulos. QBB: Quantization with Binary Bases for LLMs. In *The Thirty-eighth Annual Conference on Neural Information Processing Systems*, 2024. URL https://openreview.net/forum?id=Kw6MRGFx0R.

Jerry Chee, Yaohui Cai, Volodymyr Kuleshov, and Christopher M De Sa. QuIP: 2-Bit Quantization of Large Language Models With Guarantees. In *Advances in Neural Information Processing Systems*, volume 36, pp. 4396–4429. Curran Associates, Inc., 2023. URL https://proceedings.neurips.cc/paper_files/paper/2023/file/0df38cd13520747e1e64e5b123a78ef8-Paper-Conference.pdf.

Hong Chen, Chengtao Lv, Liang Ding, Haotong Qin, Xiabin Zhou, Yifu Ding, Xuebo Liu, Min Zhang, Jinyang Guo, Xianglong Liu, and Dacheng Tao. DB-LLM: Accurate Dual-Binarization for Efficient LLMs. In *Findings of the Association for Computational Linguistics: ACL 2024*, pp. 8719–8730, Bangkok, Thailand, August 2024. Association for Computational Linguistics. doi: 10.18653/v1/2024.findings-acl.516. URL https://aclanthology.org/2024.findings-acl.516/.

Christopher Clark, Kenton Lee, Ming-Wei Chang, Tom Kwiatkowski, Michael Collins, and Kristina Toutanova. BoolQ: Exploring the Surprising Difficulty of Natural Yes/No Questions. In *Proceedings of the 2019 Conference of the North American Chapter of the Association for Computational Linguistics: Human Language Technologies, Volume 1 (Long and Short Papers)*, pp.

2924–2936, Minneapolis, Minnesota, June 2019. Association for Computational Linguistics. doi: 10.18653/v1/N19-1300. URL https://aclanthology.org/N19-1300/.

Peter Clark, Isaac Cowhey, Oren Etzioni, Tushar Khot, Ashish Sabharwal, Carissa Schoenick, and Oyvind Tafjord. Think you have Solved Question Answering? Try ARC, the AI2 Reasoning Challenge. *arXiv preprint arXiv:1803.05457*, 2018.

Matthieu Courbariaux, Yoshua Bengio, and Jean-Pierre David. BinaryConnect: Training Deep Neural Networks with Binary Weights during Propagations. In *Advances in Neural Information Processing Systems*, volume 28. Curran Associates, Inc., 2015.

Tim Dettmers and Luke Zettlemoyer. The case for 4-bit precision: k-bit Inference Scaling Laws. In *Proceedings of the 40th International Conference on Machine Learning*, volume 202 of *Proceedings of Machine Learning Research*, pp. 7750–7774. PMLR, 23–29 Jul 2023. URL https://proceedings.mlr.press/v202/dettmers23a.html.

Tim Dettmers, Mike Lewis, Younes Belkada, and Luke Zettlemoyer. GPT3.int8(): 8-bit Matrix Multiplication for Transformers at Scale. In *Advances in Neural Information Processing Systems*, 2022. URL https://openreview.net/forum?id=dXiGWqBoxaD.

Tim Dettmers, Artidoro Pagnoni, Ari Holtzman, and Luke Zettlemoyer. QLoRA: Efficient Finetuning of Quantized LLMs. In *Advances in Neural Information Processing Systems*, volume 36, pp. 10088–10115. Curran Associates, Inc., 2023. URL https://proceedings.neurips.cc/paper_files/paper/2023/file/1feb87871436031bdc0f2beaa62a049b-Paper-Conference.pdf.

Tim Dettmers, Ruslan A. Svirschevski, Vage Egiazarian, Denis Kuznedelev, Elias Frantar, Saleh Ashkboos, Alexander Borzunov, Torsten Hoefler, and Dan Alistarh. SpQR: A Sparse-Quantized Representation for Near-Lossless LLM Weight Compression. In *The Twelfth International Conference on Learning Representations*, 2024. URL https://openreview.net/forum?id=Q1u25ahSuy.

Peijie Dong, Lujun Li, Yuedong Zhong, DaYou Du, Ruibo FAN, Yuhan Chen, Zhenheng Tang, Qiang Wang, Wei Xue, Yike Guo, and Xiaowen Chu. STBLLM: Breaking the 1-Bit Barrier with Structured Binary LLMs. In *The Thirteenth International Conference on Learning Representations*, 2025. URL https://openreview.net/forum?id=6XUSDvBFkV.

C. Eckart and G. Young. The Approximation of One Matrix by Another of Lower Rank. *Psychometrika*, 1936.

Elias Frantar, Saleh Ashkboos, Torsten Hoefler, and Dan Alistarh. OPTQ: Accurate Quantization for Generative Pre-trained Transformers. In *The Eleventh International Conference on Learning Representations*, 2023. URL https://openreview.net/forum?id=tcbBPnfwxS.

Eberhard Fuchs, Gabriele Flügge, et al. Adult Neuroplasticity: More than 40 Years of Research. *Neural plasticity*, 2014, 2014.

Robert Gray. Vector Quantization. *IEEE ASSP Magazine*, 1(2):4–29, 1984.

Andrey Gromov, Kushal Tirumala, Hassan Shapourian, Paolo Glorioso, and Dan Roberts. The Unreasonable Ineffectiveness of the Deeper Layers. In *The Thirteenth International Conference on Learning Representations*, 2025. URL https://openreview.net/forum?id=ngmEcEer8a.

Donald Olding Hebb. *The Organization of Behavior: A Neuropsychological Theory*. Psychology press, 2005.

Geoffrey Hinton, Vinyals Oriol, and Jeff Dean. Distilling the Knowledge in a Neural Network. *arXiv preprint arXiv:1503.02531*, 1, 2015.

Wei Huang, Yangdong Liu, Haotong Qin, Ying Li, Shiming Zhang, Xianglong Liu, Michele Magno, and Xiaojuan Qi. BiLLM: Pushing the Limit of Post-Training Quantization for LLMs. In *Proceedings of the 41st International Conference on Machine Learning*, volume 235 of *Proceedings of Machine Learning Research*, pp. 20023–20042. PMLR, 21–27 Jul 2024. URL https://proceedings.mlr.press/v235/huang24q.html.

Itay Hubara, Matthieu Courbariaux, Daniel Soudry, Ran El-Yaniv, and Yoshua Bengio. Binarized neural networks. In *Advances in neural information processing systems*, pp. 4107–4115, 2016.

Dongwon Jo, Taesu Kim, Yulhwa Kim, and Jae-Joon Kim. Mixture of Scales: Memory-Efficient Token-Adaptive Binarization for Large Language Models. In *The Thirty-eighth Annual Conference on Neural Information Processing Systems*, 2024. URL https://openreview.net/forum?id=pGOBEYcXzs.

Charles Jordan. *Calculus of Finite Differences*. Chelsea Publishing Company, New York, 2nd edition, 1950. doi: https://doi.org/10.1017/S0025557200230271.

Sehoon Kim, Coleman Richard Charles Hooper, Amir Gholami, Zhen Dong, Xiuyu Li, Sheng Shen, Michael W. Mahoney, and Kurt Keutzer. SqueezeLLM: Dense-and-Sparse Quantization. In *Proceedings of the 41st International Conference on Machine Learning*, volume 235 of *Proceedings of Machine Learning Research*, pp. 23901–23923. PMLR, 21–27 Jul 2024. URL https://proceedings.mlr.press/v235/kim24f.html.

Diederik P Kingma and Jimmy Ba. Adam: A Method for Stochastic Optimization. In *International Conference on Learning Representations*, 2015.

Jongwoo Ko, Sungnyun Kim, Tianyi Chen, and Se-Young Yun. DistiLLM: Towards Streamlined Distillation for Large Language Models. In *Proceedings of the 41st International Conference on Machine Learning*, volume 235 of *Proceedings of Machine Learning Research*, pp. 24872–24895. PMLR, 21–27 Jul 2024. URL https://proceedings.mlr.press/v235/ko24c.html.

Tanishq Kumar, Zachary Ankner, Benjamin Frederick Spector, Blake Bordelon, Niklas Muennighoff, Mansheej Paul, Cengiz Pehlevan, Christopher Re, and Aditi Raghunathan. Scaling Laws for Precision. In *The Thirteenth International Conference on Learning Representations*, 2025. URL https://openreview.net/forum?id=wg1PCg3CUP.

Changhun Lee, Jungyu Jin, Taesu Kim, Hyungjun Kim, and Eunhyeok Park. OWQ: Outlier-aware Weight Quantization for Efficient Fine-tuning and Inference of Large Language Models. In *Proceedings of the AAAI Conference on Artificial Intelligence*, volume 38, pp. 13355–13364, 2024.

Zhiteng Li, Xianglong Yan, Tianao Zhang, Haotong Qin, Dong Xie, Jiang Tian, Zhongchao Shi, Linghe Kong, Yulun Zhang, and Xiaokang Yang. ARB-LLM: Alternating Refined Binarizations for Large Language Models. In *The Thirteenth International Conference on Learning Representations*, 2025. URL https://openreview.net/forum?id=ZU8OdDLTts.

Ji Lin, Jiaming Tang, Haotian Tang, Shang Yang, Wei-Ming Chen, Wei-Chen Wang, Guangxuan Xiao, Xingyu Dang, Chuang Gan, and Song Han. AWQ: Activation-aware Weight Quantization for On-Device LLM Compression and Acceleration. In *Proceedings of Machine Learning and Systems*, volume 6, pp. 87–100, 2024. URL https://proceedings.mlsys.org/paper_files/paper/2024/file/42a452cbafa9dd64e9ba4aa95cc1ef21-Paper-Conference.pdf.

Aixin Liu, Bei Feng, Bing Xue, Bingxuan Wang, Bochao Wu, Chengda Lu, Chenggang Zhao, Chengqi Deng, Chenyu Zhang, Chong Ruan, et al. DeepSeek-V3 Technical Report. *arXiv preprint arXiv:2412.19437*, 2024a.

James Liu, Guangxuan Xiao, Kai Li, Jason D. Lee, Song Han, Tri Dao, and Tianle Cai. BitDelta: Your Fine-Tune May Only Be Worth One Bit. In *Advances in Neural Information Processing Systems*, volume 37, pp. 13579–13600. Curran Associates, Inc., 2024b. URL https://proceedings.neurips.cc/paper_files/paper/2024/file/187d94b3c93343f0e925b5cf729eadd5-Paper-Conference.pdf.

Zechun Liu, Barlas Oguz, Aasish Pappu, Lin Xiao, Scott Yih, Meng Li, Raghuraman Krishnamoorthi, and Yashar Mehdad. BiT: Robustly Binarized Multi-distilled Transformer. In *Advances in Neural Information Processing Systems*, volume 35, pp. 14303–14316. Curran Associates, Inc., 2022. URL https://proceedings.neurips.cc/paper_files/paper/2022/file/5c1863f711c721648387ac2ef745facb-Paper-Conference.pdf.

Zechun Liu, Barlas Oguz, Aasish Pappu, Yangyang Shi, and Raghuraman Krishnamoorthi. Binary and Ternary Natural Language Generation. In *Proceedings of the 61st Annual Meeting of the Association for Computational Linguistics (Volume 1: Long Papers)*, pp. 65–77, Toronto, Canada, 2023. Association for Computational Linguistics. doi: 10.18653/v1/2023.acl-long.5. URL https://aclanthology.org/2023.acl-long.5/.

Zechun Liu, Barlas Oguz, Changsheng Zhao, Ernie Chang, Pierre Stock, Yashar Mehdad, Yangyang Shi, Raghuraman Krishnamoorthi, and Vikas Chandra. LLM-QAT: Data-Free Quantization Aware Training for Large Language Models. In *Findings of the Association for Computational Linguistics: ACL 2024*, pp. 467–484, Bangkok, Thailand, 2024c. Association for Computational Linguistics. URL https://aclanthology.org/2024.findings-acl.26/.

Ilya Loshchilov and Frank Hutter. Decoupled Weight Decay Regularization. In *International Conference on Learning Representations*, 2019. URL https://openreview.net/forum?id=Bkg6RiCqY7.

Shuming Ma, Hongyu Wang, Lingxiao Ma, Lei Wang, Wenhui Wang, Shaohan Huang, Lifeng Dong, Ruiping Wang, Jilong Xue, and Furu Wei. The Era of 1-bit LLMs: All Large Language Models are in 1.58 Bits. *arXiv preprint arXiv:2402.17764*, 1, 2024.

Stephen Merity, Caiming Xiong, James Bradbury, and Richard Socher. Pointer Sentinel Mixture Models. In *International Conference on Learning Representations*, 2017. URL https://openreview.net/forum?id=Byj72udxe.

Ari Morcos, Maithra Raghu, and Samy Bengio. Insights on Representational Similarity in Neural Networks with Canonical Correlation. In *Advances in Neural Information Processing Systems*, volume 31. Curran Associates, Inc., 2018. URL https://proceedings.neurips.cc/paper_files/paper/2018/file/a7a3d70c6d17a73140918996d03c014f-Paper.pdf.

Van Minh Nguyen. Variation and Boolean Logic BackPropagation. *arXiv preprint arXiv:2311.07427*, 2023.

Van Minh Nguyen, Cristian Ocampo, Aymen Askri, Louis Leconte, and Ba-Hien Tran. BOLD: Boolean Logic Deep Learning. In *The Thirty-eighth Annual Conference on Neural Information Processing Systems*, 2024. URL https://openreview.net/forum?id=DO9wPZOPjk.

Adam Paszke, Sam Gross, Francisco Massa, Adam Lerer, James Bradbury, Gregory Chanan, Trevor Killeen, Zeming Lin, Natalia Gimelshein, Luca Antiga, Alban Desmaison, Andreas Kopf, Edward Yang, Zachary DeVito, Martin Raison, Alykhan Tejani, Sasank Chilamkurthy, Benoit Steiner, Lu Fang, Junjie Bai, and Soumith Chintala. PyTorch: An Imperative Style, High-Performance Deep Learning Library. In *Advances in Neural Information Processing Systems*, volume 32. Curran Associates, Inc., 2019.

Haotong Qin, Yifu Ding, Mingyuan Zhang, Qinghua YAN, Aishan Liu, Qingqing Dang, Ziwei Liu, and Xianglong Liu. BiBERT: Accurate Fully Binarized BERT. In *International Conference on Learning Representations*, 2022. URL https://openreview.net/forum?id=5xEgrl_5FAJ.

Colin Raffel, Noam Shazeer, Adam Roberts, Katherine Lee, Sharan Narang, Michael Matena, Yanqi Zhou, Wei Li, and Peter J. Liu. Exploring the Limits of Transfer Learning with a Unified Text-to-Text Transformer. *Journal of Machine Learning Research*, 21(140):1–67, 2020. URL http://jmlr.org/papers/v21/20-074.html.

Mohammad Rastegari, Vicente Ordonez, Joseph Redmon, and Ali Farhadi. XNOR-Net: ImageNet Classification Using Binary Convolutional Neural Networks. In *Proceedings of the European Conference on Computer Vision (ECCV)*, October 2016.

Keisuke Sakaguchi, Ronan Le Bras, Chandra Bhagavatula, and Yejin Choi. Winogrande: An Adversarial Winograd Schema Challenge at Scale. *Communications of the ACM*, 64(9):99–106, 2021.

Wenqi Shao, Mengzhao Chen, Zhaoyang Zhang, Peng Xu, Lirui Zhao, Zhiqian Li, Kaipeng Zhang, Peng Gao, Yu Qiao, and Ping Luo. OmniQuant: Omnidirectionally Calibrated Quantization for Large Language Models. In *The Twelfth International Conference on Learning Representations*, 2024. URL https://openreview.net/forum?id=8Wuvhh0LYW.

Ying Sheng, Lianmin Zheng, Binhang Yuan, Zhuohan Li, Max Ryabinin, Beidi Chen, Percy Liang, Christopher Re, Ion Stoica, and Ce Zhang. FlexGen: High-Throughput Generative Inference of Large Language Models with a Single GPU. In *Proceedings of the 40th International Conference on Machine Learning*, volume 202 of *Proceedings of Machine Learning Research*, pp. 31094–31116. PMLR, 23–29 Jul 2023.

Hugo Touvron, Thibaut Lavril, Gautier Izacard, Xavier Martinet, Marie-Anne Lachaux, Timothée Lacroix, Baptiste Rozière, Naman Goyal, Eric Hambro, Faisal Azhar, et al. LLaMA: Open and Efficient Foundation Language Models. *arXiv preprint arXiv:2302.13971*, 2023a.

Hugo Touvron, Louis Martin, Kevin Stone, Peter Albert, Amjad Almahairi, Yasmine Babaei, Nikolay Bashlykov, Soumya Batra, Prajjwal Bhargava, Shruti Bhosale, et al. Llama 2: Open Foundation and Fine-Tuned Chat Models. *arXiv preprint arXiv:2307.09288*, 2023b.

Albert Tseng, Jerry Chee, Qingyao Sun, Volodymyr Kuleshov, and Christopher De Sa. QuIP#: Even Better LLM Quantization with Hadamard Incoherence and Lattice Codebooks. In *Proceedings of the 41st International Conference on Machine Learning*, volume 235 of *Proceedings of Machine Learning Research*, pp. 48630–48656. PMLR, 21–27 Jul 2024a.

Albert Tseng, Qingyao Sun, David Hou, and Christopher De. QTIP: Quantization with Trellises and Incoherence Processing. In *Advances in Neural Information Processing Systems*, volume 37, pp. 59597–59620. Curran Associates, Inc., 2024b. URL https://proceedings.neurips.cc/paper_files/paper/2024/file/6de2e84b8da47bb2eb5e2ac96c63d2b0-Paper-Conference.pdf.

Ashish Vaswani, Noam Shazeer, Niki Parmar, Jakob Uszkoreit, Llion Jones, Aidan N Gomez, Ł ukasz Kaiser, and Illia Polosukhin. Attention is All you Need. In *Advances in Neural Information Processing Systems*, volume 30. Curran Associates, Inc., 2017. URL https://proceedings.neurips.cc/paper_files/paper/2017/file/3f5ee243547dee91fbd053c1c4a845aa-Paper.pdf.

Hongyu Wang, Shuming Ma, Li Dong, Shaohan Huang, Huaijie Wang, Lingxiao Ma, Fan Yang, Ruiping Wang, Yi Wu, and Furu Wei. BitNet: Scaling 1-bit Transformers for Large Language Models. *arXiv preprint arXiv:2310.11453*, 2023.

Lei Wang, Lingxiao Ma, Shijie Cao, Quanlu Zhang, Jilong Xue, Yining Shi, Ningxin Zheng, Ziming Miao, Fan Yang, Ting Cao, Yuqing Yang, and Mao Yang. Ladder: Enabling Efficient Low-Precision Deep Learning Computing through Hardware-aware Tensor Transformation. In *18th USENIX Symposium on Operating Systems Design and Implementation (OSDI 24)*, pp. 307–323, Santa Clara, CA, 2024. USENIX Association. ISBN 978-1-939133-40-3. URL https://www.usenix.org/conference/osdi24/presentation/wang-lei.

Xinghao Wang, Pengyu Wang, Bo Wang, Dong Zhang, Yunhua Zhou, and Xipeng Qiu. BitStack: Any-Size Compression of Large Language Models in Variable Memory Environments. In *The Thirteenth International Conference on Learning Representations*, 2025. URL https://openreview.net/forum?id=lBntjGbyv0.

Yuqiao Wen, Zichao Li, Wenyu Du, and Lili Mou. f-Divergence Minimization for Sequence-Level Knowledge Distillation. In *Proceedings of the 61st Annual Meeting of the Association for Computational Linguistics (Volume 1: Long Papers)*, pp. 10817–10834, Toronto, Canada, 2023. Association for Computational Linguistics. doi: 10.18653/v1/2023.acl-long.605. URL https://aclanthology.org/2023.acl-long.605/.

Yuzhuang Xu, Xu Han, Zonghan Yang, Shuo Wang, Qingfu Zhu, Zhiyuan Liu, Weidong Liu, and Wanxiang Che. OneBit: Towards Extremely Low-bit Large Language Models. In *The Thirty-eighth Annual Conference on Neural Information Processing Systems*, 2024. URL https://openreview.net/forum?id=ZwiG9KjfHV.

Zifei Xu, Sayeh Sharify, Wanzin Yazar, Tristan J Webb, and Xin Wang. Understanding the Difficulty of Low-Precision Post-Training Quantization for LLMs. In *ICLR 2025 Workshop on Sparsity in LLMs*, 2025. URL https://openreview.net/forum?id=fx9eAKwZKk.

Zhewei Yao, Reza Yazdani Aminabadi, Minjia Zhang, Xiaoxia Wu, Conglong Li, and Yuxiong He. ZeroQuant: Efficient and Affordable Post-Training Quantization for Large-Scale Transformers. In *Advances in Neural Information Processing Systems*, 2022. URL https://openreview.net/forum?id=f-fVCElZ-G1.

Haoran You, Yipin Guo, Yichao Fu, Wei Zhou, Huihong Shi, Xiaofan Zhang, Souvik Kundu, Amir Yazdanbakhsh, and Yingyan (Celine) Lin. ShiftAddLLM: Accelerating Pretrained LLMs via Post-Training Multiplication-Less Reparameterization. In *Advances in Neural Information Processing Systems*, volume 37, pp. 24822–24848. Curran Associates, Inc., 2024. URL https://proceedings.neurips.cc/paper_files/paper/2024/file/2c30a37c75f062e0bf79297c73db8c6c-Paper-Conference.pdf.

Zhihang Yuan, Yuzhang Shang, and Zhen Dong. PB-LLM: Partially Binarized Large Language Models. In *The Twelfth International Conference on Learning Representations*, 2024. URL https://openreview.net/forum?id=BifeBRhikU.

Rowan Zellers, Ari Holtzman, Yonatan Bisk, Ali Farhadi, and Yejin Choi. HellaSwag: Can a Machine Really Finish Your Sentence? In *Proceedings of the 57th Annual Meeting of the Association for Computational Linguistics*, pp. 4791–4800, Florence, Italy, 2019. Association for Computational Linguistics. doi: 10.18653/v1/P19-1472. URL https://aclanthology.org/P19-1472/.

Susan Zhang, Stephen Roller, Naman Goyal, Mikel Artetxe, Moya Chen, Shuohui Chen, Christopher Dewan, Mona Diab, Xian Li, Xi Victoria Lin, et al. OPT: Open Pre-trained Transformer Language Models. *arXiv preprint arXiv:2205.01068*, 2022.

Jiawei Zhao, Zhenyu Zhang, Beidi Chen, Zhangyang Wang, Anima Anandkumar, and Yuandong Tian. GaLore: Memory-Efficient LLM Training by Gradient Low-Rank Projection. In *Proceedings of the 41st International Conference on Machine Learning*, volume 235 of *Proceedings of Machine Learning Research*, pp. 61121–61143. PMLR, 21–27 Jul 2024. URL https://proceedings.mlr.press/v235/zhao24s.html.

Appendix

Table of Contents

A Primer on Boolean Neural Networks

For completeness, this section reviews the concepts and methodology of Boolean neural networks as proposed by Nguyen (2023); Nguyen et al. (2024).

A.1 Neuron Design

Boolean Neuron. Consider the l-th Boolean linear layer; in the forward pass, the output of the next layer is defined as Nguyen et al. (2024):

$$\mathbf{Y}^{(l)}_{[k,j]} = \mathbf{b}^{(l)}_{[j]} + \sum_{i=1}^{n} \mathrm{L}(\mathbf{X}^{(l)}_{[k,i]}, \mathbf{W}^{(l)}_{[i,j]}), \qquad 1 \le j \le m, \tag{14}$$

where k denotes the sample index in the batch, and L is a logic gate such as $\mathbf{and}$, $\mathbf{or}$, $\mathbf{xor}$, or $\mathbf{xnor}$; The weights $\mathbf{W}^{(l)}_{[i,j]}$ are Boolean values $\{\text{TRUE}, \text{FALSE}\}$ or $\{-1, +1\}$, as typically used in practical implementations. n and m are the number of input and output neurons, respectively. As the most extreme use case, the input data are also Boolean values. The above summation is understood as the counting of TRUE values. We emphasize that the framework is flexible, as it allows Boolean linear layers to be connected through activation layers, layer normalization, arithmetic layers, or other types of layers.

Mixed Boolean-Real Neuron. To enable flexible integration and coexistence of Boolean designs with real-valued components in deep models, we consider two cases of mixed-type data: (i) Boolean weights with real-valued inputs, and (ii) real-valued weights with Boolean inputs. This paper focuses on the first case. These scenarios are addressed through an extension of Boolean logic to accommodate mixed-type data. To proceed, we introduce the essential notations and definitions. Specifically, we define $\mathbb{B} \triangleq \{\text{TRUE}, \text{FALSE}\}$ as the Boolean domain, equipped with standard Boolean logic operations.

***Definition* A.1** (Three-valued logic)**.** *We define the mixed logic domain as $\mathbb{M} \triangleq \mathbb{B} \cup \{0\}$, where 0 represents an undefined or neutral value. The logic connectives in $\mathbb{M}$ are defined in alignment with standard Boolean logic, as follows. First, the negation operator is extended as: $\neg\text{TRUE} = \text{FALSE}$, $\neg\text{FALSE} = \text{TRUE}$, and $\neg 0 = 0$. Next, let L denote a generic logic connective (e.g., AND, OR). We distinguish its use in $\mathbb{M}$ and $\mathbb{B}$ by writing $\mathrm{L}_{\mathbb{M}}$ and $\mathrm{L}_{\mathbb{B}}$, respectively. The extended connective $\mathrm{L}_{\mathbb{M}}$ is defined by:*

$$\mathrm{L}_{\mathbb{M}}(a, b) = \begin{cases} \mathrm{L}_{\mathbb{B}}(a, b) & \text{for } a, b \in \mathbb{B}, \\ 0 & \text{otherwise}. \end{cases}$$

Notation A.2. Denote by $\mathbb{L}$ a logic set (e.g., $\mathbb{B}$ or $\mathbb{M}$), $\mathbb{R}$ the real set, $\mathbb{Z}$ the set of integers, $\mathbb{N}$ a numeric set (e.g., $\mathbb{R}$ or $\mathbb{Z}$), and $\mathbb{D}$ a certain set of $\mathbb{L}$ or $\mathbb{N}$.

***Definition* A.3.** *For $x \in \mathbb{N}$, its logic value denoted by x_{logic} is given as $x_{\text{logic}} = \text{TRUE} \Leftrightarrow x > 0$, $x_{\text{logic}} = \text{FALSE} \Leftrightarrow x < 0$, and $x_{\text{logic}} = 0 \Leftrightarrow x = 0$.*

***Definition* A.4.** *The magnitude of a variable x, denoted by $|x|$, is defined as follows. If $x \in \mathbb{N}$, then $|x|$ is the standard absolute value. For $x \in \mathbb{L}$, the magnitude is given by:*

$$|x| = \begin{cases} 0 & \text{if } x = 0, \\ 1 & \text{otherwise}. \end{cases}$$

***Definition* A.5** (Mixed-type logic)**.** *For L a logic connective of $\mathbb{L}$ and variables a, b, operation $c = \mathrm{L}(a, b)$ is defined such that $|c| = |a||b|$ and $c_{\text{logic}} = \mathrm{L}(a_{\text{logic}}, b_{\text{logic}})$.*

A.2 Mathematical Foundation of Boolean Variation

In this section, we present the mathematical foundation of Boolean variation which is the corner stone of the method for training Boolean weights directly within the Boolean domain, without relying on FP latent weights (Nguyen et al., 2024).

A.2.1 Boolean Variation

***Definition* A.6.** *Order relations '$<$' and '$>$' in $\mathbb{B}$ are defined as follows:*

$$\text{FALSE} < \text{TRUE}, \quad \text{TRUE} > \text{FALSE}. \tag{15}$$

***Definition* A.7.** *For $a, b \in \mathbb{B}$, the variation from a to b, denoted $\delta(a \to b)$, is defined as:*

$$\delta(a \to b) \triangleq \begin{cases} \text{TRUE}, & \text{if } b > a, \\ 0, & \text{if } b = a, \\ \text{FALSE}, & \text{if } b < a. \end{cases} \tag{16}$$

***Definition* A.8** (Type conversion)**.** *Define:*

$$\begin{aligned} &\mathrm{p} \colon \mathbb{N} \to \mathbb{L} \\ &x \mapsto \mathrm{p}(x) = \begin{cases} \text{TRUE}, & \text{if } x > 0, \\ 0, & \text{if } x = 0, \\ \text{FALSE}, & \text{if } x < 0. \end{cases} \end{aligned} \tag{17}$$

Proposition A.9. *(Nguyen, 2023; Nguyen et al., 2024) The following properties hold:*

1. *$\forall x, y \in \mathbb{N}$: $\mathrm{p}(xy) = \mathbf{xnor}(\mathrm{p}(x), \mathrm{p}(y))$.*
2. *$\forall a, b \in \mathbb{L}$: $\mathrm{e}(\mathbf{xnor}(a, b)) = \mathrm{e}(a)\,\mathrm{e}(b)$.*
3. *$\forall x, y \in \mathbb{N}$: $x = y \Leftrightarrow |x| = |y|$ and $\mathrm{p}(x) = \mathrm{p}(y)$.*

In particular, property Proposition A.9(2) implies that by the embedding map $\mathrm{e}(\cdot)$, we have:

$$(\{\text{TRUE}, \text{FALSE}\}, \mathbf{xor}) \cong (\{\pm 1\}, -\times), \tag{18}$$
$$(\{\text{TRUE}, \text{FALSE}\}, \mathbf{xnor}) \cong (\{\pm 1\}, \times), \tag{19}$$

where $\cong$ and $\times$ stand for isomorphic relation, and the real multiplication, resp. A consequence is that by $\mathrm{e}(\cdot)$, a computing sequence of pointwise XOR or XNOR, counting, and majority vote is equivalent to a sequence of pointwise multiplications and accumulation performed on the embedded data.

Proposition A.10. *The following properties hold:*

1. *$a \in \mathbb{L}$, $x \in \mathbb{N}$: $\mathbf{xnor}(a, x) = \mathrm{e}(a)x$.*
2. *$x, y \in \mathbb{N}$: $\mathbf{xnor}(x, y) = xy$.*
3. *$x \in \{\mathbb{L}, \mathbb{N}\}$, $y, z \in \mathbb{N}$: $\mathbf{xnor}(x, y + z) = \mathbf{xnor}(x, y) + \mathbf{xnor}(x, z)$.*
4. *$x \in \{\mathbb{L}, \mathbb{N}\}$, $y, \lambda \in \mathbb{N}$: $\mathbf{xnor}(x, \lambda y) = \lambda \mathbf{xnor}(x, y)$.*
5. *$x \in \{\mathbb{L}, \mathbb{N}\}$, $y \in \mathbb{N}$: $\mathbf{xor}(x, y) = -\mathbf{xnor}(x, y)$.*

Proof. The proof follows definitions A.5 and A.8.

- Following Definition A.1 we have $\forall t \in \mathbb{M}$, $\mathbf{xnor}(\text{TRUE}, t) = t$, $\mathbf{xnor}(\text{FALSE}, t) = \neg t$, and $\mathbf{xnor}(0, t) = 0$. Put $v = \mathbf{xnor}(a, x)$. We have $|v| = |x|$ and $\mathrm{p}(v) = \mathbf{xnor}(a, \mathrm{p}(x))$. Hence, $a = 0 \Rightarrow \mathrm{p}(v) = 0 \Rightarrow v = 0$; $a = \text{TRUE} \Rightarrow \mathrm{p}(v) = \mathrm{p}(x) \Rightarrow v = x$; $a = \text{FALSE} \Rightarrow \mathrm{p}(v) = \neg\,\mathrm{p}(x) \Rightarrow v = -x$. Hence (1).
- The result is trivial if $x = 0$ or $y = 0$. For $x, y \neq 0$, put $v = \mathbf{xnor}(x, y)$, we have $|v| = |x||y|$ and $\mathrm{p}(v) = \mathbf{xnor}(\mathrm{p}(x), \mathrm{p}(y))$. According to Definition A.8, if $\mathrm{sign}(x) =$

sign(y), we have $\mathrm{p}(v) = \text{TRUE} \Rightarrow v = |x||y| = xy$. Otherwise, i.e., sign$(x) = -$ sign(y), $\mathrm{p}(v) = \text{FALSE} \Rightarrow v = -|x||y| = xy$. Hence (2).

- (3) and (4) follow (1) for $x \in \mathbb{L}$ and follow (2) for $x \in \mathbb{N}$.
- For (5), write $u = \mathbf{xor}(x, y)$ and $v = \mathbf{xnor}(x, y)$, we have $|u| = |v|$ and $\mathrm{p}(u) = \mathbf{xor}(\mathrm{p}(x), \mathrm{p}(y)) = \neg\mathbf{xnor}(\mathrm{p}(x), \mathrm{p}(y)) = \neg\, \mathrm{p}(v)$. Thus, $\mathrm{sign}(u) = -\,\mathrm{sign}(v) \Rightarrow u = -v$. □

Notation A.11. We denote $\mathcal{F}(\mathbb{S}, \mathbb{T})$ the set of all functions from source $\mathbb{S}$ to image $\mathbb{T}$.

***Definition* A.12.** *For $f \in \mathcal{F}(\mathbb{B}, \mathbb{D})$, $\forall x \in \mathbb{B}$, write $\delta f(x \to \neg x) := \delta(f(x) \to f(\neg x))$. The variation of f w.r.t. x, denoted $f'(x)$, is defined as:*

$$f'(x) \triangleq \mathbf{xnor}(\delta(x \to \neg x), \delta f(x \to \neg x)).$$

Remark A.13. For convenience and consistency of notation, we intentionally adopt the standard symbol for the continuous derivative, f', to also denote Boolean variation The intended meaning — whether it represents a continuous derivative or a Boolean variation — can be inferred from the context in which the function f is defined. Intuitively, the variation of f w.r.t x is TRUE if f varies in the same direction with x.

Example A.14. Let $a \in \mathbb{B}$, $f(x) = \mathbf{xor}(x, a)$ for $x \in \mathbb{B}$, the variation of f w.r.t. x can be derived by establishing a truth table (see Table 4) from which we obtain $f'(x) = \neg a$.

Table 4: Variation truth table of $f(x) = \mathbf{xor}(a, x)$, $a, x \in \mathbb{B}$.

a	x	$\neg x$	$\delta(x \to \neg x)$	$f(a, x)$	$f(a, \neg x)$	$\delta f(x \to \neg x)$	$f'(x)$
TRUE	TRUE	FALSE	FALSE	FALSE	TRUE	TRUE	FALSE
TRUE	FALSE	TRUE	TRUE	TRUE	FALSE	FALSE	FALSE
FALSE	TRUE	FALSE	FALSE	TRUE	FALSE	FALSE	TRUE
FALSE	FALSE	TRUE	TRUE	FALSE	TRUE	TRUE	TRUE

A.2.2 Boolean Variation Calculus

Below are some rules of Boolean variation which are necessary for training Boolean neural networks.

Proposition A.15. *(Nguyen, 2023; Nguyen et al., 2024) For $f, g \in \mathcal{F}(\mathbb{B}, \mathbb{B})$, $\forall x, y \in \mathbb{B}$ the following properties hold:*

1. $\delta f(x \to y) = \mathbf{xnor}(\delta(x \to y), f'(x))$.
2. $(\neg f(x))' = \neg f'(x)$.
3. $(g \circ f)'(x) = \mathbf{xnor}(g'(f(x)), f'(x))$.

Proof. The proof is by definition:

1. $\forall x, y \in \mathbb{B}$, there are two cases. If $y = x$, then the result is trivial. Otherwise, i.e., $y = \neg x$, by definition we have:

$$\begin{aligned} & f'(x) = \mathbf{xnor}(\delta(x \to \neg x), \delta f(x \to \neg x)) \\ \Leftrightarrow \quad & \delta f(x \to \neg x) = \mathbf{xnor}(\delta(x \to \neg x), f'(x)). \end{aligned}$$

Hence the result.

2. $\forall x, y \in \mathbb{B}$, it is easy to verify by truth table that $\delta(\neg f(x \to y)) = \neg\delta f(x \to y)$. Hence, by definition,

$$\begin{aligned}(\neg f)'(x) &= \mathbf{xnor}(\delta(x \to \neg x), \delta(\neg f(x \to \neg x)))\\ &= \mathbf{xnor}(\delta(x \to \neg x), \neg\delta f(x \to \neg x))\\ &= \neg\mathbf{xnor}(\delta(x \to \neg x), \delta f(x \to \neg x))\\ &= \neg f'(x).\end{aligned}$$

3. Using definition, property (i), and associativity of **xnor**, $\forall x \in \mathbb{B}$ we have:

$$\begin{aligned}(g \circ f)'(x) &= \mathbf{xnor}(\delta(x \to \neg x), \delta g(f(x) \to f(\neg x)))\\ &= \mathbf{xnor}(\delta(x \to \neg x), \mathbf{xnor}(\delta f(x \to \neg x), g'(f(x))))\\ &= \mathbf{xnor}(g'(f(x)), \mathbf{xnor}(\delta(x \to \neg x), \delta f(x \to \neg x)))\\ &= \mathbf{xnor}(g'(f(x)), f'(x)).\end{aligned}$$

□

Proposition A.16. *(Nguyen, 2023; Nguyen et al., 2024) For $f \in \mathcal{F}(\mathbb{B}, \mathbb{N})$, the following properties hold:*

1. *$x, y \in \mathbb{B}$: $\delta f(x \to y) = \mathbf{xnor}(\delta(x \to y), f'(x))$.*
2. *$\alpha \in \mathbb{N}$: $(\alpha f)'(x) = \alpha f'(x)$.*
3. *$g \in \mathcal{F}(\mathbb{B}, \mathbb{N})$: $(f + g)'(x) = f'(x) + g'(x)$.*

Proof. The proof is as follows:

1. For $x, y \in \mathbb{B}$. Firstly, the result is trivial if $y = x$. For $y \neq x$, i.e., $y = \neg x$, by definition:

$$f'(x) = \mathbf{xnor}(\delta(x \to \neg x), \delta f(x \to \neg x)).$$

Hence, $|\delta f(x \to \neg x)| = |f'(x)|$ since $|\delta(x \to \neg x)| = 1$, and

$$\begin{aligned}&\mathrm{p}(f'(x)) = \mathbf{xnor}(\delta(x \to \neg x), \mathrm{p}(\delta f(x \to \neg x)))\\ \Leftrightarrow\quad &\mathrm{p}(\delta f(x \to \neg x)) = \mathbf{xnor}(\delta(x \to \neg x), \mathrm{p}(f'(x))),\end{aligned}$$

where $\mathrm{p}(\cdot)$ is the logic projector Eq. 17. Thus, $\delta f(x \to \neg x) = \mathbf{xnor}(\delta(x \to \neg x), f'(x))$. Hence the result.

2. Firstly $\forall x, y \in \mathbb{B}$, we have

$$\delta(\alpha f(x \to y)) = \alpha f(y) - \alpha f(x) = \alpha\delta f(x \to y).$$

Hence, by definition,

$$\begin{aligned}(\alpha f)'(x) &= \mathbf{xnor}(\delta(x \to \neg x), \delta(\alpha f(x \to \neg x)))\\ &= \mathbf{xnor}(\delta(x \to \neg x), \alpha\delta f(x \to \neg x))\\ &= \alpha\,\mathbf{xnor}(\delta(x \to \neg x), \delta f(x \to \neg x)), \text{ due to Proposition A.10(4)}\\ &= \alpha f'(x).\end{aligned}$$

3. For $f, g \in \mathcal{F}(\mathbb{B}, \mathbb{N})$,

$$\begin{aligned}(f + g)'(x) &= \mathbf{xnor}(\delta(x \to \neg x), \delta(f + g)(x \to \neg x))\\ &= \mathbf{xnor}(\delta(x \to \neg x), \delta f(x \to \neg x) + \delta g(x \to \neg x))\\ &\overset{(*)}{=} \mathbf{xnor}(\delta(x \to \neg x), \delta f(x \to \neg x)) + \mathbf{xnor}(\delta(x \to \neg x), \delta g(x \to \neg x)),\\ &= f'(x) + g'(x),\end{aligned}$$

where $(*)$ is due to Proposition A.10(3). □

For $f \in \mathcal{F}(\mathbb{Z}, \mathbb{N})$, its derivative, also known in terms of *finite differences*, has been defined in the literature as $f'(x) = f(x+1) - f(x)$, see e.g. Jordan (1950). With the logic variation as introduced above, we can make this definition more generic as follows.

***Definition* A.17.** *For $f \in \mathcal{F}(\mathbb{Z}, \mathbb{D})$, the variation of f w.r.t $x \in \mathbb{Z}$ is defined as $f'(x) \triangleq \delta f(x \to x+1)$, where δf is in the sense of the variation defined in $\mathbb{D}$.*

Proposition A.18. *(Nguyen, 2023; Nguyen et al., 2024) The following composition rules (chain rules) hold:*

1. *For $\mathbb{B} \xrightarrow{f} \mathbb{B} \xrightarrow{g} \mathbb{D}$: $(g \circ f)'(x) = \mathbf{xnor}(g'(f(x)), f'(x))$, $\forall x \in \mathbb{B}$.*
2. *For $\mathbb{B} \xrightarrow{f} \mathbb{Z} \xrightarrow{g} \mathbb{D}$, $x \in \mathbb{B}$, if $|f'(x)| \leq 1$ and $g'(f(x)) = g'(f(x)-1)$, then:*
$$(g \circ f)'(x) = \mathbf{xnor}(g'(f(x)), f'(x)).$$

Proof. The proof is as follows.

1. The case of $\mathbb{B} \xrightarrow{f} \mathbb{B} \xrightarrow{g} \mathbb{B}$ is obtained from Proposition A.15(3). For $\mathbb{B} \xrightarrow{f} \mathbb{B} \xrightarrow{g} \mathbb{N}$, by using Proposition A.16(1), the proof is similar to that of Proposition A.15(3).

2. By definition, we have
$$(g \circ f)'(x) = \mathbf{xnor}(\delta(x \to \neg x), \delta g(f(x) \to f(\neg x))). \tag{20}$$
Using property (1) of Proposition A.16, we have:
$$\begin{aligned} f(\neg x) &= f(x) + \delta f(x \to \neg x) \\ &= f(x) + \mathbf{xnor}(\delta(x \to \neg x), f'(x)). \end{aligned} \tag{21}$$
Applying Eq. 21 back to Eq. 20, the result is trivial if $f'(x) = 0$. The remaining case is $|f'(x)| = 1$ for which we have $\mathbf{xnor}(\delta(x \to \neg x), f'(x)) = \pm 1$. First, for $\mathbf{xnor}(\delta(x \to \neg x), f'(x)) = 1$, we have:
$$\begin{aligned} \delta g(f(x) \to f(\neg x)) &= \delta g(f(x) \to f(x)+1) \\ &= g'(f(x)) \\ &= \mathbf{xnor}(g'(f(x)), 1) \\ &= \mathbf{xnor}(g'(f(x)), \mathbf{xnor}(\delta(x \to \neg x), f'(x))). \end{aligned} \tag{22}$$
Substitute Eq. 22 back to Eq. 20, we obtain:
$$\begin{aligned} (g \circ f)'(x) &= \mathbf{xnor}(\delta(x \to \neg x), \delta g(f(x) \to f(\neg x))) \\ &= \mathbf{xnor}(\delta(x \to \neg x), \mathbf{xnor}(g'(f(x)), \mathbf{xnor}(\delta(x \to \neg x), f'(x)))) \\ &= \mathbf{xnor}(g'(f(x)), f'(x)), \end{aligned}$$
where that last equality is by the associativity of $\mathbf{xnor}$ and that $\mathbf{xnor}(x, x) = \text{True}$ for $x \in \mathbb{B}$. Similarly, for $\mathbf{xnor}(\delta(x \to \neg x), f'(x)) = -1$, we have:
$$\begin{aligned} \delta g(f(x) \to f(\neg x)) &= \delta g(f(x) \to f(x)-1) \\ &= -g'(f(x)-1) \\ &= \mathbf{xnor}(g'(f(x)-1), -1) \\ &= \mathbf{xnor}(g'(f(x)-1), \mathbf{xnor}(\delta(x \to \neg x), f'(x))). \end{aligned} \tag{23}$$
Substitute Eq. 23 back to Eq. 20 and use the assumption that $g'(f(x)) = g'(f(x)-1)$, we have:
$$\begin{aligned} (g \circ f)'(x) &= \mathbf{xnor}(\delta(x \to \neg x), \delta g(f(x) \to f(\neg x))) \\ &= \mathbf{xnor}(\delta(x \to \neg x), \mathbf{xnor}(g'(f(x)-1), \mathbf{xnor}(\delta(x \to \neg x), f'(x)))) \\ &= \mathbf{xnor}(g'(f(x)), f'(x)). \end{aligned}$$
Hence the preposition is proved. □

Example A.19. From Example A.14, we have $\delta\mathbf{xor}(x, a)/\delta x = \neg a$ for $a, x \in \mathbb{B}$. Using Proposition A.15-(2) we have: $\delta\mathbf{xnor}(x, a)/\delta x = a$ since $\mathbf{xnor}(x, a) = \neg\mathbf{xor}(x, a)$.

A.2.3 Multivariate Case

The properties of Boolean variation described above can be extended to the multivariate case in a straightforward manner. For example, in the case of multivariate Boolean functions, the extension is as follows.

***Definition* A.20.** *For $\mathbf{x} = (x_1, \dots, x_n) \in \mathbb{B}^n$, denote $\mathbf{x}_{\neg i} \triangleq (x_1, \dots, x_{i-1}, \neg x_i, x_{i+1}, \dots, x_n)$ for $n \geq 1$ and $1 \leq i \leq n$. For $f \in \mathcal{F}(\mathbb{B}^n, \mathbb{B})$, the (partial) variation of f w.r.t. x_i, denoted $f'_i(\mathbf{x})$ or $\delta f(\mathbf{x})/\delta x_i$, is defined as: $f'_i(\mathbf{x}) \equiv \delta f(\mathbf{x})/\delta x_i \triangleq \mathbf{xnor}(\delta(x_i \to \neg x_i), \delta f(\mathbf{x} \to \mathbf{x}\neg i))$.*

The composition rule then becomes:

Proposition A.21. *(Nguyen et al., 2024) Let $f \in \mathcal{F}(\mathbb{B}^n, \mathbb{B})$, $n \geq 1$, and $g \in \mathcal{F}(\mathbb{B}, \mathbb{B})$. For $1 \leq i \leq n$:*

$$(g \circ f)'_i(\mathbf{x}) = \mathbf{xnor}(g'(f(\mathbf{x})), f'_i(\mathbf{x})), \quad \forall \mathbf{x} \in \mathbb{B}^n. \tag{24}$$

Example A.22. Apply Proposition A.16-(3) to $\mathbf{Y}^{(l)}_{[k,j]}$ from Eq. 14: $\delta \mathbf{Y}^{(l)}_{[k,j]}/\delta \mathbf{W}^{(l)}_{[i,j]} = \delta \mathrm{L}(\mathbf{X}^{(l)}_{[k,i]}, \mathbf{W}^{(l)}_{[i,j]})/\delta \mathbf{W}^{(l)}_{[i,j]}$ and $\delta \mathbf{Y}^{(l)}_{[k,j]}/\delta \mathbf{X}^{(l)}_{[k,i]} = \delta \mathrm{L}(\mathbf{X}^{(l)}_{[k,i]}, \mathbf{W}^{(l)}_{[i,j]})/\delta \mathbf{X}^{(l)}_{[k,i]}$. Then, for $\mathrm{L} = \mathbf{xnor}$ as an example, we have: $\delta \mathbf{Y}^{(l)}_{[k,j]}/\delta \mathbf{W}^{(l)}_{[i,j]} = \mathbf{X}^{(l)}_{[k,i]}$ and $\delta \mathbf{Y}^{(l)}_{[k,j]}/\delta \mathbf{X}^{(l)}_{[k,i]} = \mathbf{W}^{(l)}_{[i,j]}$.

A.3 Boolean Backpropagation

This section presents how to apply the above principles of Boolean variation to define backpropagation for Boolean neural networks. The l-th layer (Eq. 14), receives the backpropagation signal from the downstream layer $l+1$. Specifically, $\mathbf{Z}^{(l)}_{[k,j]} \triangleq \frac{\delta \mathcal{L}}{\delta \mathbf{Y}^{(l)}_{[k,j]}}$ denotes the variation of the loss function $\mathcal{L}$ w.r.t. the output at layer l. To optimize the Boolean weights, we need to compute the corresponding loss signal, denoted as $\mathbf{Q}^{(l)}_{[i,j]} \triangleq \frac{\delta \mathcal{L}}{\delta \mathbf{W}^{(l)}_{[i,j]}}$. In addition, we also have to compute the loss signal for the upstream layer, defined as $\mathbf{P}^{(l)}_{[k,i]} \triangleq \frac{\delta \mathcal{L}}{\delta \mathbf{X}^{(l)}_{[k,i]}}$. Hereafter, we consider the logic gate $\mathrm{L} = \mathbf{xnor}$ as a concrete example.

First, using Proposition A.15, Proposition A.16, Proposition A.18 and its extension to the multivariate case by Proposition A.21 in the same manner as shown in Example A.22, we have:

$$\frac{\delta \mathbf{Y}^{(l)}_{[k,j]}}{\delta \mathbf{W}^{(l)}_{[i,j]}} = \frac{\delta \mathbf{xnor}(\mathbf{X}^{(l)}_{[k,i]}, \mathbf{W}^{(l)}_{[i,j]})}{\delta \mathbf{W}^{(l)}_{[i,j]}} = \mathbf{X}^{(l)}_{[k,i]} \tag{25}$$

$$\frac{\delta \mathbf{Y}^{(l)}_{[k,j]}}{\delta \mathbf{X}^{(l)}_{[k,i]}} = \frac{\delta \mathbf{xnor}(\mathbf{X}^{(l)}_{[k,i]}, \mathbf{W}^{(l)}_{[i,j]})}{\delta \mathbf{X}^{(l)}_{[k,i]}} = \mathbf{W}^{(l)}_{[i,j]} \tag{26}$$

Using the chain rules given by Proposition A.18, we have the following atomic variations:

$$\mathbf{Q}^{(l)}_{[k,i,j]} \triangleq \frac{\delta \mathcal{L}}{\delta \mathbf{W}^{(l)}_{[i,j]}}|_k = \mathbf{xnor}\left(\frac{\delta \mathcal{L}}{\delta \mathbf{Y}^{(l)}_{[k,j]}}, \frac{\delta \mathbf{Y}^{(l)}_{[k,j]}}{\delta \mathbf{W}^{(l)}_{[i,j]}}\right) = \mathbf{xnor}\left(\mathbf{Z}^{(l)}_{[k,j]}, \mathbf{X}^{(l)}_{[k,i]}\right), \tag{27}$$

$$\mathbf{P}^{(l)}_{[k,i,j]} \triangleq \frac{\delta \mathcal{L}}{\delta \mathbf{X}^{(l)}_{[k,i]}}|_j = \mathbf{xnor}\left(\frac{\delta \mathcal{L}}{\delta \mathbf{Y}^{(l)}_{[k,j]}}, \frac{\delta \mathbf{Y}^{(l)}_{[k,j]}}{\delta \mathbf{X}^{(l)}_{[k,i]}}\right) = \mathbf{xnor}\left(\mathbf{Z}^{(l)}_{[k,j]}, \mathbf{W}^{(l)}_{[i,j]}\right). \tag{28}$$

The variations $\mathbf{Q}^{(l)}_{[i,j]}$ and $\mathbf{G}^{(l)}_{[k,i]}$ can be then obtained by aggregating the above atomic variations over the batch dimension k and output dimension j, respectively. More specifically, denote $\mathbf{1}(\cdot)$ the indicator function. Additionally, for $b \in \mathbb{B}$ and a variable x, we define $\mathbf{1}(x = b) = 1$ if $x_{\text{logic}} = b$

and $\mathbf{1}(x = b) = 0$ otherwise. Then, we have:

$$\mathbf{Q}^{(l)}_{[i,j]} \triangleq \frac{\delta \mathcal{L}}{\delta \mathbf{W}^{(l)}_{[i,j]}} = \sum_k \mathbf{1}(\mathbf{Q}^{(l)}_{[k,i,j]} = \text{TRUE})|\mathbf{Q}^{(l)}_{[k,i,j]}| - \sum_k \mathbf{1}(\mathbf{Q}^{(l)}_{[k,i,j]} = \text{FALSE})|\mathbf{Q}^{(l)}_{[k,i,j]}|, \tag{29}$$

$$\mathbf{P}^{(l)}_{[i,j]} \triangleq \frac{\delta \mathcal{L}}{\delta \mathbf{X}^{(l)}_{[k,i]}} = \sum_j \mathbf{1}(\mathbf{P}^{(l)}_{[k,i,j]} = \text{TRUE})|\mathbf{P}^{(l)}_{[k,i,j]}| - \sum_j \mathbf{1}(\mathbf{P}^{(l)}_{[k,i,j]} = \text{FALSE})|\mathbf{P}^{(l)}_{[k,i,j]}|. \tag{30}$$

A.4 Boolean Optimizer

Algorithm 1: Boolean learning process for a linear layer.

```
Input      : Learning rate $\eta$, number of iterations $T$;
Initialize : $\mathbf{M}^{(l),0}_{[i,j]} = 0$; $\beta^0 = 1$;
1  for $t = 0, \dots, T-1$ do
       /* 1. Forward */
2      Compute $\mathbf{Y}^{(l),t}$ following Eq. 14;
       /* 2. Backward */
3      Receive $\frac{\delta \mathcal{L}}{\delta \mathbf{Y}^{(l),t}_{[k,j]}}$ from downstream layer;
       /* 2.1 Backpropagation */
4      Compute and backpropagate $\mathbf{P}^{(l),t}$ to the upstream following Eq. 30;
       /* 2.2 Weight update process */
5      $N_{\text{total}} := 0$, $N_{\text{unchanged}} := 0$;
6      foreach $\mathbf{W}^{l}_{i,j}$ do
7          Compute $\mathbf{Q}^{(l),t+1}_{[i,j]}$ following Eq. 29;
8          Update $\mathbf{M}^{(l),t+1}_{[i,j]} = \beta^t \mathbf{M}^{(l),t}_{[i,j]} + \eta^t \mathbf{Q}^{(l),t+1}_{[i,j]}$;
9          $N_{\text{total}} \leftarrow N_{\text{total}} + 1$;
10         if xnor$(\mathbf{M}^{(l),t+1}_{[i,j]}, \mathbf{W}^{(l),t}_{[i,j]}) = \text{TRUE}$ then
               /* Flip weight */
11             $\mathbf{W}^{(l),t+1}_{[i,j]} = \neg \mathbf{W}^{(l),t}_{[i,j]}$;
               /* Reset corresponding accumulator */
12             $\mathbf{M}^{(l),t+1}_{[i,j]} = 0$;
13         else
               /* Weight is unchanged */
14             $\mathbf{W}^{(l),t+1}_{[i,j]} = \mathbf{W}^{(l),t}_{[i,j]}$;
               /* Update statistics to update $\beta$ */
15             $N_{\text{unchanged}} \leftarrow N_{\text{unchanged}} + 1$;
16     Update $\eta^{t+1}$, $\beta^{t+1} = N_{\text{unchanged}} / N_{\text{total}}$ ;
```

Given the above variations, the rule for updating the Boolean weight $\mathbf{W}^{(l)}_{[i,j]}$ to minimize the loss function $\mathcal{L}$ is as follows:

$$\mathbf{W}^{(l)}_{[i,j]} = \neg \mathbf{W}^{(l)}_{[i,j]} \quad \text{if } \mathbf{xnor}\left(\mathbf{Q}^{(l)}_{[i,j]}, \mathbf{W}^{(l)}_{[i,j]}\right) = \text{TRUE}. \tag{31}$$

Based on this update rule, we can develop an optimizer that accumulates the signal $\mathbf{Q}^{(l)}_{[i,j]}$ over training iterations. Specifically, let $\mathbf{W}^{(l),t}_{[i,j]}$ denotes the weight at iteration t, and $\mathbf{M}^{(l),t}_{[i,j]}$ represents its accumulator, initialized as $\mathbf{M}^{(l),0}_{[i,j]} = 0$. The update rule for the accumulator is then defined as: The update rule for the accumulator is then defined as:

$$\mathbf{M}^{(l),t+1}_{[i,j]} \leftarrow \beta^t \mathbf{M}^{(l),t}_{[i,j]} + \eta \mathbf{Q}^{(l),t}_{[i,j]}, \tag{32}$$

where η is the accumulation factor acting as a learning rate, and β^t is an auto-regularizing factor that reflects the system's state at time t. In our work, we use brain plasticity (Fuchs et al., 2014) and Hebbian theory (Hebb, 2005) to adaptively set β^t, that force the weights to adapt to their neighborhood during. For the chose weight's neighborhood, for instance, neuron, layer, or network level, β^t is set as:

$$\beta^t = \frac{\text{Number of unchanged weights at } t}{\text{Total number of weights}}. \tag{33}$$

It to temper the importance of weight variational according to how much neurons have changed. In our experiments, β^t is set to per-layer basis and initialized as $\beta^0 = 1$ The learning process for a linear layer is described in Algorithm 1.

B Discussion on Hardware Considerations

B.1 Computation Proposed in § 4.1

The Boolean framework supports both full and partial binary settings. The afforementioned Boolean variation calculus shows that:

$$\mathbf{xnor}(x_{\text{real}}, w_{\text{logic}}) = x_{\text{real}} \times w_{\text{binary}}, \tag{34}$$

under the mapping TRUE $\to +1$ and FALSE $\to -1$. Consequently, matrix multiplication ($\mathbf{matmul}$) between a real tensor $\mathbf{X}$ and a logic tensor $\mathbf{W}$ can be implemented as follows:

- **Using binary weights** $\{-1, +1\}$: Simply represent the logic weights in binary format. Then, $\mathbf{matmul}(x_{\text{real}}, w_{\text{logic}})$ is directly computed as $\mathbf{matmul}(x_{\text{real}}, w_{\text{binary}})$.
- **Using native logic** $\{\text{TRUE}, \text{FALSE}\}$: The multiplication reduces to:

$$\mathbf{matmul}(x_{\text{real}}, w_{\text{logic}}) = \begin{cases} x_{\text{real}}, & \text{if } w_{\text{logic}} = \text{TRUE} \\ -x_{\text{real}}, & \text{if } w_{\text{logic}} = \text{FALSE} \end{cases} \tag{35}$$

  Thus, a sign flip of x_{real} conditioned on w_{logic}, followed by accumulation, suffices to perform $\mathbf{matmul}(\mathbf{X}_{\text{real}}, \mathbf{W}_{\text{logic}})$.

The first approach is well-supported by modern hardware such as CPUs, GPUs, etc, where different bit-widths can be used to represent and simulate weight values in $\{-1, +1\}$. Additionally, this approach can be implemented directly in PyTorch (Paszke et al., 2019). The second approach, in contrast, requires a specialized Boolean accelerator. Such hardware can massively accelerate the computation by directly leveraging logic operations instead of real-arithmetic.

B.2 Multi-core Computation Strategy in § 4.2

Boolean design, as used in the paper, employs Boolean weights and operates using logic operations. It is distinct from bit-level operations.

Boolean design: Weights are Boolean logic variables, taking values TRUE/FALSE or $-1/+1$. Operations are logic-based, such as **xnor**, and **or**, etc. See Eq. 35 for an example.

Bit-level operations: These, such as bit-serial implementations in C/C++, operate bit-by-bit on multi-bit variables. For instance, a bit-level AND between two n-bit variables produces an n-bit result, where each bit is the ADN of corresponding pair of bits from the inputs. Bit-level operations like bit-serial are inefficient in terms of latency, whereas Boolean logic operations are significantly faster compared to real-arithmetic operations such as multiplication.

C Code Samples of Core Implementation

C.1 Boolean Linear Layer and Optimizer

In this section, we provide example Python code for implementing a Boolean linear layer based on the **xor** logic gate. This implementation is based on the PyTorch framework (Paszke et al., 2019). As done in Nguyen et al. (2024), the class definition for the Boolean linear layer is presented in Algorithm 2, and its backpropagation mechanism—customized via PyTorch's `autograd` system—is detailed in Algorithm 3. Each Boolean kernel is primarily implemented using this Boolean linear layer.

We consider both cases of the incoming backpropagation signal: Boolean-valued (see Algorithm 4), and real-valued (see Algorithm 5). The latter is the main use case in this paper. An example implementation of the Boolean optimizer used to update the layer's parameters is provided in Algorithm 6.

Algorithm 2: Python code of XOR linear layer

```python
import torch

from torch import Tensor, nn, autograd
from typing import Any, List, Optional, Callable


class XORLinear(nn.Linear):

    def __init__(self, in_features: int, out_features: int, bool_bprop: bool, **kwargs):
        super(XORLinear, self).__init__(in_features, out_features, **kwargs)
        self.bool_bprop = bool_bprop

    def reset_parameters(self):
        self.weight = nn.Parameter(torch.randint(0, 2, self.weight.shape))

        if self.bias is not None:
            self.bias = nn.Parameter(torch.randint(0, 2, (self.out_features,)))

    def forward(self, X):
        return XORFunction.apply(X, self.weight, self.bias, self.bool_bprop)
```

Algorithm 3: Python code of the backpropagation logic of XOR linear layer

```python
class XORFunction(autograd.Function):

    @staticmethod
    def forward(ctx, X, W, B, bool_bprop: bool):
        ctx.save_for_backward(X,W,B)
        ctx.bool_bprop = bool_bprop

        # Elementwise XOR logic
        S = torch.logical_xor(X[:,None,:], W[None,:,:])

        # Sum over the input dimension
        S = S.sum(dim=2) + B

        # 0-centered for use with BatchNorm when preferred
        S = S - W.shape[1]/2

        return S

    @staticmethod
    def backward(ctx, Z):
        if ctx.bool_bprop:
            G_X, G_W, G_B = backward_bool(ctx, Z)
        else:
            G_X, G_W, G_B = backward_real(ctx, Z)

        return G_X, G_W, G_B, None
```

Algorithm 4: Backpropagation logic with Boolean received backpropagation

```
def backward_bool(ctx, Z):
    """
    Variation of input:
        - delta(xor(x,w))/delta(x) = neg w
        - delta(Loss)/delta(x) = xnor(z,neg w) = xor(z,w)
    Variation of weights:
        - delta(xor(x,w))/delta(w) = neg x
        - delta(Loss)/delta(x) = xnor(z,neg x) = xor(z,x)
    Variation of bias:
        - bias = xnor(bias,True) ==> Variation of bias is driven in
          the same basis as that of weight with xnor logic and input True.
    Aggregation:
        - Count the number of TRUEs = sum over the Boolean data
        - Aggr = TRUEs - FALSEs = TRUEs - (TOT - TRUEs) = 2TRUES - TOT
          where TOT is the size of the aggregated dimension
    """
    X, W, B = ctx.saved_tensors

    # Boolean variation of input
    G_X = torch.logical_xor(Z[:,:,None], W[None,:,:])

    # Aggregate over the out_features dimension
    G_X = 2 * G_X.sum(dim=1) - W.shape[0]

    # Boolean variation of weights
    G_W = torch.logical_xor(Z[:,:,None], X[:,None,:])

    # Aggregate over the batch dimension
    G_W = 2 * G_W.sum(dim=0) - X.shape[0]

    # Boolean variation of bias
    if B is not None:
        # Aggregate over the batch dimension
        G_B = 2 * Z.sum(dim=0) - Z.shape[0]

    # Return
    return G_X, G_W, G_B
```

Algorithm 5: Backpropagation logic with real received backpropagation

```
def backward_real(ctx, Z):
    X, W, B = ctx.saved_tensors

    """
    Boolean variation of input processed using torch avoiding loop:
        -> xor(Z: Real, W: Boolean) = -Z * emb(W)
        -> emb(W): T->1, F->-1 => emb(W) = 2W-1
        => delta(Loss)/delta(X) = Z*(1-2W) """
    G_X = Z.mm(1-2*W)

    """
    Boolean variation of weights processed using torch avoiding loop:
        -> xor(Z: Real, X: Boolean) = -Z * emb(X)
        -> emb(X): T->1, F->-1 => emb(X) = 2X-1
        => delta(Loss)/delta(W) = Z^T * (1-2X) """
    G_W = Z.t().mm(1-2*X)

    """ Boolean variation of bias """
    if B is not None:
        G_B = Z.sum(dim=0)

    # Return
    return G_X, G_W, G_B
```

Algorithm 6: Python code of Boolean optimizer

```python
class BooleanOptimizer(torch.optim.Optimizer):

    def __init__(self, params, lr: float):
        super(BooleanOptimizer, self).__init__(params, dict(lr=lr))
        for param_group in self.param_groups:
            param_group['accums'] = [torch.zeros_like(p.data) for p in param_group['params']]
            param_group['ratios'] = [0 for p in param_group['params']]
        self._nb_flips = 0

    @property
    def nb_flips(self):
        n = self._nb_flips
        self._nb_flips = 0
        return n

    def step(self):
        for param_group in self.param_groups:
            for idx, p in enumerate(param_group['params']):
                self.update(p, param_group, idx)

    def update(self, param: Tensor, param_group: dict, idx: int):
        accum = param_group['ratios'][idx] * param_group['accums'][idx] + param_group['lr'] * param.grad.data
        param_group['accums'][idx] = accum
        param_to_flip = accum * (2*param.data-1) >= 1
        param.data[param_to_flip] = torch.logical_not(param.data[param_to_flip])
        param_group['accums'][idx][param_to_flip] = 0.
        param_group['ratios'][idx] = 1 - param_to_flip.float().mean()
        self._nb_flips += float(param_to_flip.float().sum())
```

C.2 Successive SVID for Kernel Extraction

Algorithm 7 illustrate the Python code of the SVID algortithm to extract the optimal Boolean weights and scaling factors for one kernel. Based on this, Algorithm 8 illustrates the succesive SVID algorithm to extract all kernels.

Algorithm 7: Python code of SVID approximation of a FP matrix.

```python
def svid_approximation(w):
    """
    Approximate the input matrix `w` by a boolean matrix and a rank-1 matrix:
        w = w_bool * (s_out * s_in.T)

    Args:
        w (torch.Tensor): Input tensor of shape (*, m, n).

    Returns:
        tuple:
            - w_bool (torch.Tensor): Boolean matrix of the same shape as `w`.
            - w_res (torch.Tensor): Residual matrix, w - w_bool * (s_out * s_in.T).
            - s_in (torch.Tensor): Scaled first left singular vector of `w`.
            - s_out (torch.Tensor): Scaled first right singular vector of `w`.
    """
    U, S, Vh = torch.linalg.svd(abs(w.data.clone().float()), full_matrices=False)

    w_bool = torch.sign(w)
    s_in = torch.sqrt(S[0]) * Vh[0,:].reshape(1,-1)
    s_out = torch.sqrt(S[0]) * U[:,0].reshape(-1,1)

    w_res = w - w_bool * torch.matmul(s_out, s_in)

    return w_bool, w_res, s_in, s_out
```

Algorithm 8: Python code of successively extracts kernels from FP matrix using SVID.

```python
def successive_svid(w_fp, n_kernels):
    """
    Perform successive SVID on the input matrix to extract Boolean kernels.

    Args:
        w_fp (torch.Tensor): Input weight matrix.
        n_kernels (int): Number of iterations to extract kernels.

    Returns:
        list: List of dictionaries containing `n_kernels` kernels, each has:
            - w_bool (torch.Tensor): Boolean matrix.
            - s_in (torch.Tensor): Input scaling vector.
            - s_out (torch.Tensor): Output scaling vector.
    """
    boolean_kernels = []

    w = w_fp # The input to SVID at first iteration is the original weight

    for k in range(n_kernels):
        # Extract the Boolean weights, residual, and scaling vectors
        w_bool, w_res, s_in, s_out = svid_approximation(w)

        # Save the extracted kernel
        boolean_kernels.append({'w_bool': w_bool, 's_in': s_in, 's_out': s_out})

        # The input to SVID for the next iteration is the current residual matrix
        w = w_res

    return boolean_kernels
```

D Proof of Propositions

For completeness, we include the proofs of Propositions related to SVID approximation used in the main paper.

D.1 Proof of Boolean Linear Reformulation using SVID

Proposition D.1. *(Xu et al., 2024) Given the weight matrix $\mathbf{W}_{\text{FP}}$ and input $\mathbf{X}$, the linear layer can be reformulated as the following using SVID approximation, $\mathbf{W}_{\text{FP}} \approx \mathbf{W}_{\text{bool}} \odot \left(\mathbf{s}_{\text{out}}\mathbf{s}_{\text{in}}^\top\right)$, as follows:*

$$\mathbf{X}\mathbf{W}_{\text{FP}}^\top \approx \left[\left(\mathbf{X} \odot \mathbf{s}_{\text{in}}^\top\right)\mathbf{W}_{\text{bool}}^\top\right] \odot \mathbf{s}_{\text{out}}^\top. \tag{36}$$

Proof. Due to the SVID approximation, we have $\mathbf{W}_{\text{FP}[i,j]} \approx \mathbf{W}_{\text{bool}[i,j]}\mathbf{s}_{\text{out}[i]}\mathbf{s}_{\text{in}[j]}$. Then, we have:

$$\begin{aligned}
\left(\mathbf{X}\mathbf{W}_{\text{FP}}^\top\right)_{[i,j]} &\approx \sum_k \mathbf{X}_{[i,k]}\mathbf{W}_{\text{FP}[k,j]}^\top && (37)\\
&= \sum_k \mathbf{X}_{[i,k]}\mathbf{W}_{\text{FP}[j,k]} && (38)\\
&= \sum_k \mathbf{X}_{[i,k]}\mathbf{W}_{\text{bool}[j,k]}\mathbf{s}_{\text{out}[j]}\mathbf{s}_{\text{in}[k]} && (39)\\
&= \sum_k \mathbf{X}_{[i,k]}\mathbf{s}_{\text{in}[k]}\mathbf{W}_{\text{bool}[j,k]}\mathbf{s}_{\text{out}[j]} && (40)\\
&= \sum_k \left(\mathbf{X} \odot \mathbf{s}_{\text{in}}^\top\right)_{[i,k]}\mathbf{W}_{\text{bool}[k,j]}^\top\mathbf{s}_{\text{out}[j]} && (41)\\
&= \left[\left(\mathbf{X} \odot \mathbf{s}_{\text{in}}^\top\right)\mathbf{W}_{\text{bool}}^\top\right]_{[i,j]}\mathbf{s}_{\text{out}[j]} && (42)\\
&= \left\{\left[\left(\mathbf{X} \odot \mathbf{s}_{\text{in}}^\top\right)\mathbf{W}_{\text{bool}}^\top\right] \odot \mathbf{s}_{\text{out}}^\top\right\}_{[i,j]}. && (43)
\end{aligned}$$

Thus, the proposition is proved. □

D.2 Proof of Proposition 4.1

Lemma D.2. *(Xu et al., 2024) Denote $\sigma_i(\mathbf{W})$ the i-th biggest singular value of matrix $\mathbf{W}$. The following inequality holds:*

$$\sigma_1(|\mathbf{W}|) \geq \sigma_1(\mathbf{W}). \tag{44}$$

Proof. By the definition of induced norm, we have:

$$\sigma_1(\mathbf{W}) = \|\mathbf{W}\|_2 = \max_{\mathbf{x}, \|\mathbf{x}\|_2=1} \|\mathbf{W}\mathbf{x}\|_2, \tag{45}$$

$$\sigma_1(|\mathbf{W}|) = \||\mathbf{W}|\|_2 = \max_{\mathbf{y}, \|\mathbf{y}\|_2=1} \||\mathbf{W}|\mathbf{y}\|_2. \tag{46}$$

In addition, because $\forall \mathbf{x}$, $\|\mathbf{x}\|_2 = 1$, we have:

$$\begin{aligned}
\||\mathbf{W}||\mathbf{x}|\|_2^2 &= \sum_i \left(\sum_j |\mathbf{W}_{[i,j]}||\mathbf{x}_{[j]}| \right)^2 & (47)\\
&\geq \sum_i \left(|\sum_j \mathbf{W}_{[i,j]}\mathbf{x}_{[j]}| \right)^2 & (48)\\
&= \sum_i \left(\sum_j \mathbf{W}_{[i,j]}\mathbf{x}_{[j]} \right)^2 & (49)\\
&= \|\mathbf{W}\mathbf{x}\|_2^2. & (50)
\end{aligned}$$

Therefore

$$\max_{\mathbf{y}, \|\mathbf{y}\|_2=1} \||\mathbf{W}|\mathbf{y}\|_2 \geq \max_{\mathbf{x}, \|\mathbf{x}\|_2=1} \|\mathbf{W}\mathbf{x}\|_2 \tag{51}$$

$$\Leftrightarrow \sigma_1(|\mathbf{W}|) \geq \sigma_1(\mathbf{W}). \tag{52}$$

Thus, the lemma is proved. □

Proposition D.3 (Restated from Xu et al. (2024))**.** *For $\mathbf{W} \in \mathbb{R}^{m\times n}$, write $\mathbf{W} = \widetilde{\mathbf{U}}\widetilde{\mathbf{\Sigma}}\widetilde{\mathbf{V}}^\top$ its* SVD*. Let $\mathbf{a} = \sqrt{\tilde{\sigma}_1}\widetilde{\mathbf{U}}_{[:,1]}$, and $\mathbf{b} = \sqrt{\tilde{\sigma}_1}\widetilde{\mathbf{V}}_{[:,1]}$. Similarly, denote $|\mathbf{W}| = \mathbf{U}\mathbf{\Sigma}\mathbf{V}^\top$ its* SVD*; $\mathbf{s}_{\text{in}}$ and $\mathbf{s}_{\text{out}}$ are given as: $\mathbf{s}_{\text{in}} = \sqrt{\sigma_1}\mathbf{V}_{[:,1]}$, and $\mathbf{s}_{\text{out}} = \sqrt{\sigma_1}\mathbf{U}_{[:,1]}$. We decompose the matrix as $\mathbf{W} = \mathbf{W}_{\text{bool}} \odot |\mathbf{W}| \approx \mathbf{W}_{\text{bool}} \odot \left(\mathbf{s}_{\text{out}}\mathbf{s}_{\text{in}}^\top\right)$. We then have:*

$$\left\|\mathbf{W} - \mathbf{W}_{\text{bool}} \odot \mathbf{s}_{\text{out}}\mathbf{s}_{\text{in}}^\top\right\|_F^2 \leq \left\|\mathbf{W} - \mathbf{a}\mathbf{b}^\top\right\|_F^2. \tag{53}$$

Proof. We denote the following error matrices:

$$\mathbf{E}_1 = \mathbf{W} - \mathbf{a}\mathbf{b}^\top, \tag{54}$$

$$\mathbf{E}_2 = |\mathbf{W}| - \mathbf{s}_{\text{out}}\mathbf{s}_{\text{in}}^\top. \tag{55}$$

Multiplying $\mathbf{W}_{\text{bool}}$ with both sides of Eq. 55, we have:

$$\mathbf{W}_{\text{bool}} \odot |\mathbf{W}| - \mathbf{W}_{\text{bool}} \odot \mathbf{s}_{\text{out}}\mathbf{s}_{\text{in}}^\top = \mathbf{W}_{\text{bool}} \odot \mathbf{E}_2 \tag{56}$$

$$\Leftrightarrow \mathbf{W} - \mathbf{W}_{\text{bool}} \odot \mathbf{s}_{\text{out}}\mathbf{s}_{\text{in}}^\top = \mathbf{W}_{\text{bool}} \odot \mathbf{E}_2. \tag{57}$$

Thus, we have:

$$\|\mathbf{W} - \mathbf{W}_{\text{bool}} \odot \mathbf{s}_{\text{out}}\mathbf{s}_{\text{in}}^{\top}\|_F^2 = \|\mathbf{W}_{\text{bool}} \odot \mathbf{E}_2\|_F^2 \tag{58}$$

$$= \sum_{i,j} \mathbf{W}_{\text{bool}[i,j]}^2 + \mathbf{E}_{2[i,j]}^2 \tag{59}$$

$$= \sum_{i,j} \mathbf{E}_{2[i,j]}^2 \tag{60}$$

$$= \|\mathbf{E}_2\|_F^2 \tag{61}$$

For SVD decomposition, the norm of the above error matrices in the rank-1 approximation is the um of squares of all singular values except the largest one. In particular, we have:

$$\|\mathbf{E}_1\|_F^2 = \sum_{i=2}^{n} \sigma_i^2(\mathbf{W}), \tag{62}$$

$$\|\mathbf{E}_2\|_F^2 = \sum_{i=2}^{n} \sigma_i^2(|\mathbf{W}|). \tag{63}$$

Since $\|\mathbf{W}\|_F^2 = \||\mathbf{W}|\|_F^2$, we have:

$$\sum_{i=1}^{n} \sigma_i^2(\mathbf{W}) = \sum_{i=1}^{n} \sigma_i^2(|\mathbf{W}|) \tag{64}$$

$$\Leftrightarrow \|\mathbf{E}_1\|_F^2 + \sigma_1^2(\mathbf{W}) = \|\mathbf{E}_2\|_F^2 \sigma_1^2(|\mathbf{W}|). \tag{65}$$

Thus, according to Lemma D.2 and Eq. 61, we have:

$$\|\mathbf{E}_2\|_F^2 \leq \|\mathbf{E}_1\|_F^2 \tag{66}$$

$$\left\|\mathbf{W} - \mathbf{W}_{\text{bool}} \odot \mathbf{s}_{\text{out}}\mathbf{s}_{\text{in}}^{\top}\right\|_F^2 \leq \left\|\mathbf{W} - \mathbf{a}\mathbf{b}^{\top}\right\|_F^2. \tag{67}$$

Thus, the proposition is proved. □

D.3 Proof of Proposition 4.3

Proposition D.4. *For $\mathbf{W} \in \mathbb{R}^{m \times n}$, we denote $|\mathbf{W}| = \mathbf{U}\mathbf{\Sigma}\mathbf{V}^{\top}$ its SVD. $\mathbf{s}_{\text{in}}$ and $\mathbf{s}_{\text{out}}$ are given as: $\mathbf{s}_{\text{in}} = \sqrt{\sigma_1}\mathbf{V}_{[:,1]}$, and $\mathbf{s}_{\text{out}} = \sqrt{\sigma_1}\mathbf{U}_{[:,1]}$. We decompose the matrix as $\mathbf{W} = \mathbf{W}_{\text{bool}} \odot |\mathbf{W}| \approx \mathbf{W}_{\text{bool}} \odot \left(\mathbf{s}_{\text{out}}\mathbf{s}_{\text{in}}^{\top}\right)$. We then have:*

$$\left\|\mathbf{W} - \mathbf{W}_{\text{bool}} \odot \mathbf{s}_{\text{out}}\mathbf{s}_{\text{in}}^{\top}\right\|_F^2 \leq \left\|\mathbf{W} - \mathbf{W}_{\text{bool}} \odot \mathbf{c}\mathbf{d}^{\top}\right\|_F^2, \quad \forall \mathbf{c} \in \mathbb{R}^{m \times 1}, \forall \mathbf{d} \in \mathbb{R}^{n \times 1}. \tag{68}$$

Proof. Similar to the proof of Proposition 4.3, we denote the following error matrices $\mathbf{E}_1 = |\mathbf{W}| - \mathbf{s}_{\text{out}}\mathbf{s}_{\text{in}}^{\top}$ and $\mathbf{E}_2 = |\mathbf{W}| - \mathbf{c}\mathbf{d}^{\top}$. We have that

$$\mathbf{W}_{\text{bool}} \odot |\mathbf{W}| - \mathbf{W}_{\text{bool}} \odot \mathbf{s}_{\text{out}}\mathbf{s}_{\text{in}}^{\top} = \mathbf{W}_{\text{bool}} \odot \mathbf{E}_1 \tag{69}$$

$$\Leftrightarrow \mathbf{W} - \mathbf{W}_{\text{bool}} \odot \mathbf{s}_{\text{out}}\mathbf{s}_{\text{in}}^{\top} = \mathbf{W}_{\text{bool}} \odot \mathbf{E}_1. \tag{70}$$

Therefore,

$$\left\|\mathbf{W} - \mathbf{W}_{\text{bool}} \odot \mathbf{s}_{\text{out}}\mathbf{s}_{\text{in}}^{\top}\right\|_F^2 = \|\mathbf{W}_{\text{bool}} \odot \mathbf{E}_1\|_F^2 = \sum_{i,j} \mathbf{W}_{\text{bool}[i,j]}^2 \mathbf{E}_{1[i,j]}^2 = \sum_{i,j} \mathbf{E}_{1[i,j]}^2 = \|\mathbf{E}_1\|_F^2. \tag{71}$$

Similarly, we have that

$$\left\|\mathbf{W} - \mathbf{W}_{\text{bool}} \odot \mathbf{a}\mathbf{b}^{\top}\right\|_F^2 = \|\mathbf{E}_2\|_F^2. \tag{72}$$

Thus, we need to show that

$$\|\mathbf{E}_1\|_F^2 \leq \|\mathbf{E}_2\|_F^2 \tag{73}$$

Additionally, we denote the rank-k approximation to $|\mathbf{W}|$ by SVD as $\mathbf{S}_k$:

$$\mathbf{S}_k = \sum_{i=1}^{k} \sigma_i \mathbf{U}_{[:,i]} \mathbf{V}_{[:,i]}^\top. \tag{74}$$

With this notation, we have that $\mathbf{S}_1 = \mathbf{s}_{\text{out}}\mathbf{s}_{\text{in}}^\top$ is the rank-1 approximation of $|\mathbf{W}|$ by SVD.

From Eq. 73, we need to show that if there is an arbitrary rank-1 approximation to $|\mathbf{W}|$, $\mathbf{P}_1 = \mathbf{c}\mathbf{d}^\top$, we then have

$$\left\||\mathbf{W}| - \mathbf{s}_{\text{out}}\mathbf{s}_{\text{in}}^\top\right\|_F^2 \leq \left\||\mathbf{W}| - \mathbf{c}\mathbf{d}^\top\right\|_F^2. \tag{75}$$

This can be done by using the Eckart-Young-Mirsky theorem (Eckart & Young, 1936). First, we have that

$$\||\mathbf{W}| - \mathbf{S}_1\|_F^2 = \left\||\mathbf{W}| - \mathbf{s}_{\text{out}}\mathbf{s}_{\text{in}}^\top\right\|_F^2 = \left\|\sum_{i=2}^{n} \sigma_i \mathbf{U}_{[:,i]} \mathbf{V}_{[:,i]}^\top\right\|_F^2 = \sum_{i=2}^{n} \sigma_i^2. \tag{76}$$

By the triangle inequality with the spectral norm, if $|\mathbf{W}| = \mathbf{C} + \mathbf{D}$ then $\sigma_1(|\mathbf{W}|) \leq \sigma_1(\mathbf{C}) + \sigma_1(\mathbf{D})$. Suppose the $\mathbf{C}_k$ and $\mathbf{D}_k$ denote the rank-k approximation to $\mathbf{C}$ and $\mathbf{D}$ by SVD method, respectively. Then, for any $i, j \geq 1$ we have

$$\begin{aligned}
\sigma_i(\mathbf{C}) + \sigma_j(\mathbf{D}) &= \sigma_1(\mathbf{C} - \mathbf{C}_{i-1}) + \sigma_1(\mathbf{D} - \mathbf{D}_{j-1}) && (77)\\
&\geq \sigma_1(|\mathbf{W}| - \mathbf{C}_{i-1} - \mathbf{D}_{j-1}) && (78)\\
&\geq \sigma_1(|\mathbf{W}| - \mathbf{S}_{i+j-2}) \quad (\text{since } \operatorname{rank}(\mathbf{C}_{i-1} + \mathbf{D}_{j-1}) \leq i + j - 2) && (79)\\
&= \sigma_{i+j-1}(|\mathbf{W}|). && (80)
\end{aligned}$$

Because $\sigma_2(\mathbf{P}_1) = 0$, when $\mathbf{C} = |\mathbf{W}| - \mathbf{P}_1$ and $\mathbf{D} = \mathbf{P}_1$ we have that for $i \geq 1, j = 2$, $\sigma_i(|\mathbf{W}| - \mathbf{P}_1) \geq \sigma_{i+1}(|\mathbf{W}|)$. As a result,

$$\begin{aligned}
\||\mathbf{W}| - \mathbf{P}_1\|_F^2 = \sum i = 1^n \sigma_i(|\mathbf{W}| - \mathbf{P}_1)^2 \geq \sum i = 2^n \sigma_i(|\mathbf{W}|)^2 = \||\mathbf{W}| - \mathbf{S}_1\|_F^2 && (81)\\
\Leftrightarrow \|\mathbf{E}_2\|_F^2 \geq \|\mathbf{E}_1\|_F^2 && (82)\\
\Leftrightarrow \left\|\mathbf{W} - \mathbf{W}_{\text{bool}} \odot \mathbf{c}\mathbf{d}^\top\right\|_F^2 \geq \left\|\mathbf{W} - \mathbf{W}_{\text{bool}} \odot \mathbf{s}_{\text{out}}\mathbf{s}_{\text{in}}^\top\right\|_F^2. && (83)
\end{aligned}$$

Hence the proposition is proved. □

E Details on Kernel Allocation

E.1 Weight Importance Estimation

We assess the importance of a linear weight in the original FP model by comparing the representations at its input and output. Let $\mathbf{X} \in \mathbb{R}^{d\times n}$ and $\mathbf{Y} \in \mathbb{R}^{d\times m}$ denote the input and output matrices of a linear layer, respectively, where d is the number of samples, and n and m are the input and output feature dimensions. We hypothesize that a weight is important if it significantly transforms the input representations. For example, a weight matrix equivalent to the identity does not alter the representations and thus would be considered unimportant. To quantify this transformation, we use a robust metric for comparing neural representations.

Various similarity measures can be used for this purpose, such as cosine similarity, as done in (Gromov et al., 2025). In this work, we adopt PWCCA Morcos et al. (2018), which is particularly well-suited for our setting: it is invariant to linear transformations—an essential property given that large language models (LLMs) are primarily composed of linear layers—and effectively captures shared structure while filtering out noise Morcos et al. (2018).

Specifically, we define the importance score as:

$$h = 1 - \frac{1}{c}\sum_{i=1}^{c} \rho_{\mathrm{PWCCA},i}(\mathbf{X}, \mathbf{Y}), \tag{84}$$

where c denotes the number of canonical vectors used in the comparison (typically, $c = \min(n, m)$). The matrices $\mathbf{X}$ and $\mathbf{Y}$ are obtained by simply forwarding a set of data samples through the network. In our experiments, we use 128 random samples from the WikiText2 training set to estimate the importance score. Here, $\rho_{\mathrm{PWCCA},i}$ represents the projection-weighted correlation along the i-th canonical direction. The following section describes in detail how this correlation is computed.

Algorithm 9: Kernel allocation.

```
1  Input
2      $T \geq 1$ ;                                                      /* model expansion limit */
3      $\mathbf{E} = [e_l^{[k]}] \in \mathbb{R}^{N_\mathbf{W}\times K_{\max}}$ for $k \in [1, K_{\max}], l \in [1, N_\mathbf{W}]$ ;  /* residual approx error */
4      $\mathbf{h} = [h_l] \in \mathbb{R}^{N_\mathbf{W}\times 1}$ ;                                   /* weight importance scores */
5      $\mathbf{p} = [p_l] \in \mathbb{R}^{N_\mathbf{W}\times 1}$ ;                                   /* weight size ratios */
6  Initialize
7      $\mathbf{k} = [1, \dots, 1]^\mathrm{T}$ of length $N_\mathbf{W}$ ;                              /* starting choice */
8      $\mathbf{f} = \mathbf{k} < K_{\max}$ ;                                             /* feasible indicator */
9      $\mathbf{C} = \left(\frac{1}{\mathbf{p}} \log \frac{1}{\mathbf{p}}\right) \odot \mathbf{h} \odot \mathbf{E}$ ;        /* where $\odot$ is broadcasted over $\mathbf{E}$ columns */
10 While not all $\mathbf{f}$ is False do
11     $\mathbf{g} := \emptyset, \mathbf{l} := \emptyset$;
12     for $l = 1 : N_\mathbf{W}$ do
13         if $\mathbf{f}[l]$ = True then
14             $g := \mathbf{C}[l, \mathbf{k}[l]] - \mathbf{C}[l, \mathbf{k}[l] + 1]$ ;   /* gain by increasing kernel size by 1 */
15             Append $l$ to $\mathbf{l}$, append $g$ to $\mathbf{g}$;
16     Sort $\mathbf{g}$ in decreasing order, and arrange $\mathbf{l}$ accordingly;
17     for $(g, l)$ in $(\mathbf{g}, \mathbf{l})$ do
18         $\mathbf{k}_l := \mathbf{k}$;
19         $\mathbf{k}_l[l] = \mathbf{k}_l[l] + 1$;
20         if $\mathbf{k}_l^\mathrm{T}\mathbf{p} \leq T$ then
21             $\mathbf{k}[l] = \mathbf{k}[l] + 1$;
22             break ;                                                 /* escape the for loop */
23         else
24             $\mathbf{f}[l]$ := False;
25     $\mathbf{f} \leftarrow$ and$(\mathbf{f}, \mathbf{k} < K_{\max})$ ;                      /* element-wise logical and */
26 return $\mathbf{k}$
```

Projection-weighted Canonical Correlation Analysis. Canonical Correlation Analysis (CCA) finds bases for two matrices such that, when the original matrices are projected onto these bases, the resulting projections are maximally correlated. Without loss of generality, we assume that $n \leq m$. For $1 \leq i \leq n$, the i-th canonical correlation coefficient ρ_i is given by:

$$\begin{aligned} \rho_i = \max_{\mathbf{w}^i_{\mathbf{X}}, \mathbf{w}^i_{\mathbf{Y}}} & \operatorname{corr}(\mathbf{X}\mathbf{w}^i_{\mathbf{X}}, \mathbf{Y}\mathbf{Y}\mathbf{w}^i_{\mathbf{Y}}) \\ \text{subject to } & \mathbf{X}\mathbf{w}^i_{\mathbf{X}} \perp \mathbf{X}\mathbf{w}^j_{\mathbf{X}} \quad \forall j < i \\ & \mathbf{Y}\mathbf{w}^i_{\mathbf{Y}} \perp \mathbf{Y}\mathbf{w}^j_{\mathbf{Y}} \quad \forall j < i. \end{aligned} \tag{85}$$

The vectors $\mathbf{w}^i_{\mathbf{X}} \in \mathbb{R}^n$ and $\mathbf{w}^i_{\mathbf{Y}} \in \mathbb{R}^m$ that maximize ρ_i are called the canonical weights. These weights transform the original data into the canonical variables $\mathbf{X}\mathbf{w}^i_{\mathbf{X}}$ and $\mathbf{Y}\mathbf{w}^i_{\mathbf{Y}}$. The constraints in Eq. 85 enforce orthogonality among the canonical variables, ensuring that each successive pair captures a distinct mode of correlation.

The mean CCA correlation is then computed as:

$$\bar{\rho}_{\text{CCA}} = \frac{\sum_{i=1}^{n} \rho_i}{n}, \tag{86}$$

where n is the number of canonical correlation coefficients considered.

CCA is sensitive to perturbation when the condition number of $\mathbf{X}$ and $\mathbf{Y}$ is large. To imporve robustness, Morcos et al. (2018) propose a strategy to reduce this sensitivity, which they term "projection-weighted CCA" (PWCCA).

$$\rho_{\text{PWCCA},i} = \frac{\sum_{i=1}^{c} \alpha_i \rho_i}{\sum_{i=1}^{c} \alpha_i}, \quad \alpha_i = \sum_j |\langle \mathbf{h}_i, \mathbf{x}_j \rangle|, \tag{87}$$

where $\mathbf{x}_j$ is the j-th column of $\mathbf{X}$, and $\mathbf{h}_i = \mathbf{X}\mathbf{w}^i_{\mathbf{X}}$ is the vector of canonical variables formed by projecting $\mathbf{X}$ to the i-th canonical cooridate frame.

E.2 Kernel Allocation Algorithm

Algorithm 9 illustrates the details of our algorithm for kernel allocation.

F Theoretical Analysis of Training Complexity

Consider a linear layer without bias, defined as $\mathbf{Y} = \mathbf{X}\mathbf{W}$ where $\mathbf{X} \in \mathbb{R}^{B \times L \times N}$ and $\mathbf{W} \in \mathbb{R}^{N \times M}$. Here, B is the mini-batch size, L is the sequence length, N is the input dimension, and M is the output dimension. We analyze the number of multiplications (MULs) required.

Latent-weight approach (same cost as full-precision training):

- Forward: $B \times L \times N \times M$ (FP16–FP16 MULs)
- Backward w.r.t. weights: $B \times L \times N \times M$ (FP16–FP16 MULs)
- Backward w.r.t. inputs: $B \times L \times N \times M$ (FP16–FP16 MULs)
- **Total:** $3 \times B \times L \times N \times M$ FP16–FP16 MULs

Boolean approach with K kernels: (assuming FP16 gradients for a fair comparison). As shown in the main text, only the final Boolean kernel needs to be fine-tuned. The number of multiplications becomes:

- Forward: $K \times B \times L \times N \times M$ (BOOL–FP16 MULs, using all K kernels)
- Backward w.r.t. weights: $1 \times B \times L \times N \times M$ (FP16–FP16 MULs, for last kernel only)
- Backward w.r.t. inputs: $1 \times B \times L \times N \times M$ (BOOL–FP16 MULs, for last kernel only)
- **Total:** $(K + 1) \times B \times L \times N \times M$ BOOL–FP16 MULs, and $B \times L \times N \times M$ FP16–FP16 MULs

Since K is typically small (e.g., 2–4) while B and L are large (thousands), most computation shifts from FP16–FP16 to the more efficient BOOL–FP16 operations. If we ignore the BOOL–FP16 MULs, the FP16–FP16 operations are reduced by a factor of $2/3$ (i.e., a 66.7% reduction). Remarkably, this reduction is achieved while using more kernels and attaining better performance, yet with significantly lower training complexity. According to BitNet (Wang et al., 2023) (Table 1), for $L = 512$ and a LLaMA-like 13B model on 7 nm hardware, 1Bit–FP16 operations yield an energy saving of approximately **56**$\times$ compared to FP16–FP16. Hence, our method achieves substantial training efficiency. Importantly, BitNet is a latent-weight approach, with efficiency gains realized primarily during inference, whereas our method provides significant benefits already during training and fine-tuning.

We note that the above analysis does not include optimizer cost. The latent-weight approach typically relies on Adam, which requires two full-precision momenta per parameter and a complex update rule involving multiple normalization statistics. By contrast, our Boolean approach employs a Boolean optimizer requiring only one full-precision momentum per parameter, coupled with a much simpler update rule (see Eq. 3). This further underscores the reduction in overall training complexity offered by our method.

G Additional Experiemental Results

G.1 Additional Information of Experiemental Settings

We use 12 Nvidia GPUs of Tesla V100 for our experiments. We follow exactly the experimental settings in Jo et al. (2024). The results of the baselines in Table 2 are taken from Xu et al. (2024); Jo et al. (2024).

G.2 On the Choice of KD Loss

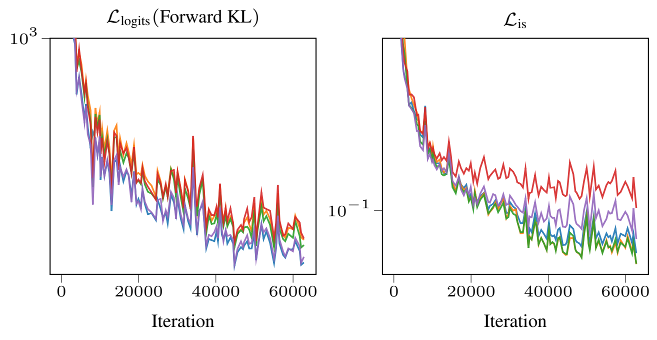

D_{logits}	Wiki2	C4
🟦 Forward KL	**31.39**	**28.50**
🟧 Reverse KL	33.14	29.46
🟩 Symmetric KL	32.67	29.26
🟥 JS Divergence	31.78	28.69
🟪 TV Distance	33.02	29.56

Figure 12: The training convergence of $\mathcal{L}_{\text{is}}$, and $\mathcal{L}_{\text{logits}}$, measured by Forward KL, and the final results with respect to the choice of D_{logits}.

Fig. 12 illustrates the convergence and results of using different choices for D_{logits} in Eq. 10. Despite its simplicity, forward KL achieves the best performance. More complex measures, such as total variance (TV) distance (Wen et al., 2023) and Jensen-Shannon (JS) divergence (Agarwal et al., 2024), offer no significant benefits in our case. Furthermore, we observe that the final perplexity is strongly correlated with $\mathcal{L}_{\text{logits}}$ using forward KL, but not with $\mathcal{L}_{\text{is}}$, as shown in Fig. 12 and Fig. 6. As a result, we employ the forward KL in all experiments.

G.3 Results of Different Number of Kernels on LLMs

To complement the Table 2, Table 5 shows the benchmarking results of LLMs using our MBOK method with varying numbers of kernels per weight. Consistent with the observations made on smaller models in § 6.1.1, we observe that increasing the number of kernels generally improves performance. However, the performance gains begin to diminish noticeably beyond three kernels.

Table 5: Perplexity and zero-shot accuracy results of our MBOK method with different number of kernels.

Model	Method	Wbits	Perplexity (↓) Wiki2	C4	Zero-shot Accuracy (↑) BoolQ	PIQA	Hella.	WinoG.	ARC-e	ARC-c	Average
OPT-1.3B	MBOK (2 kernels)	2×1	16.13	16.61	58.53	70.67	48.11	56.75	48.19	27.90	51.69
	MBOK (3 kernels)	3×1	15.30	15.68	60.64	70.78	50.71	56.83	48.82	28.49	52.71
	MBOK (4 kernels)	4×1	**14.83**	**14.92**	60.95	70.85	51.02	56.85	49.13	29.24	**53.01**
LLaMA-7B	MBOK (2 kernels)	2×1	6.83	8.53	69.20	74.32	64.80	60.30	49.05	34.90	58.76
	MBOK (3 kernels)	3×1	6.20	7.76	67.89	76.15	68.91	63.30	48.94	37.62	60.47
	MBOK (4 kernels)	4×1	**6.01**	**7.53**	68.16	76.71	69.85	62.09	49.24	38.14	**60.70**
LLaMA-13B	MBOK (2 kernels)	2×1	6.17	7.88	68.10	76.33	69.88	64.17	52.34	37.88	61.45
	MBOK (3 kernels)	3×1	5.58	7.15	67.39	77.74	73.37	66.61	54.04	41.21	63.39
	MBOK (4 kernels)	4×1	**5.38**	**6.91**	68.69	77.63	74.23	66.53	56.14	41.38	**64.10**

G.4 Additional Results on LLaMA-2

Table 6 shows the results on LLaMA2-13B (Touvron et al., 2023b). Similar to the Table 2, the results of the baselines are taken from Xu et al. (2024) and Jo et al. (2024). It is clear that our method consistently outperforms the baselines across different metrics and model sizes.This further emphasizes the robustness of our approach across various types of models.

Table 6: Perplexity and zero-shot accuracy results of Float16, quantized and binarized LLaMA2 models.

Model	Method	Wbits	Perplexity (↓) Wiki2	C4	Zero-shot Accuracy (↑) BoolQ	PIQA	Hella.	WinoG.	ARC-e	ARC-c	Average
LLaMA2-7B	FP16	16	5.47	6.97	71.10	76.88	72.94	67.09	53.58	40.61	63.70
	PB-LLM	1.7	76.75	85.92	62.17	52.82	26.87	50.11	26.89	24.31	40.53
	BiLLM	1.11	27.72	36.34	62.14	59.19	35.18	53.11	34.22	26.54	45.06
	OneBit	1	8.60	10.74	63.06	70.40	54.24	56.67	40.82	29.35	52.42
	MoS	1	7.88	9.75	65.02	71.55	59.41	56.18	41.84	30.03	54.01
	OPTQ	2	7.7e3	NaN	42.97	49.46	26.19	50.28	26.77	28.58	37.38
	LLM-QAT	2	1.1e3	6.6e2	59.14	50.12	25.10	49.08	26.26	26.96	35.89
	OmniQuant	2	31.21	64.34	58.69	56.53	33.87	51.22	33.63	24.32	43.12
	MBOK [Ours]	2×1	**6.87**	**8.74**	66.94	74.97	65.59	61.72	44.82	34.21	**58.04**
	MBOK [Ours]	3×1	**6.12**	**7.81**	65.46	75.79	69.59	62.04	49.11	37.80	**59.97**
LLaMA2-13B	FP16	16	4.88	6.47	68.99	79.05	76.62	69.77	57.95	44.20	66.10
	PB-LLM	1.7	155.25	151.15	37.82	53.26	28.89	49.48	28.28	23.72	36.91
	BiLLM	1.11	20.71	27.19	62.20	62.51	38.05	56.35	40.69	27.73	47.92
	OneBit	1	7.56	9.67	65.66	71.60	60.07	56.91	45.76	31.74	55.29
	MoS	1	7.08	8.91	66.12	73.72	63.80	58.98	45.71	33.19	57.09
	OPTQ	2	2.1e3	3.2e2	40.61	51.74	25.67	51.85	25.46	27.30	37.11
	LLM-QAT	2	5.1e2	1.1e3	39.85	49.08	24.37	51.38	27.15	24.32	36.03
	OmniQuant	2	16.88	27.02	62.05	62.24	50.34	53.20	40.66	29.61	49.68
	MBOK [Ours]	2×1	**5.97**	**7.85**	66.32	75.84	70.24	62.51	50.00	37.46	**60.40**
	MBOK [Ours]	3×1	**5.35**	**7.07**	66.80	77.59	73.79	65.27	54.47	41.89	**63.30**

G.5 Generation Quality

Table 7 illustrates the generated text given zero-shot arbitrary questions from LLaMA-13B with FP16 weights and MBOK using three kernels. It is clearly that our model is able to produce meaningful and coherennt text compared to the original FP16 model.

Table 7: Comparison of generation quality (*non-curated*) on LLaMA-13B models with FP16 and MBOK using three kernels.

Prompt:	What are the capitals of China, US and Russia?
FP16:	The capital of China is Beijing. The capital of the United States is Washington D.C. and the capital of Russia is Moscow.
MBOK:	The capital of China is Beijing. The capital of the US is Washington D.C. and the capital of Russia is Moscow.
Prompt:	I have a friend who lives in London and I would like to visit him. How would I go there from Paris?
FP16:	You can take the Eurostar from Gare du Nord in Paris to St. Pancras Station in London. The trip takes about 2 hours and 15 minutes.
MBOK:	The fastest way to get from Paris to London is to take the Eurostar train. The Eurostar departs from the Gare du Nord station in Paris and arrives at the St. Pancras International station in London. The trip takes about 2 hours and 15 minutes.
Prompt:	What is Fete du Travail?
FP16:	It is an annual holiday celebrated all over the world that resulted from the labour union movement, to celebrate the economic and social achievements of workers. The majority of countries celebrate Labour Day on May Day, or May 1, and it is popularly known as May Day and International Workers' Day
MBOK:	In France, May 1st is a public holiday. It is also known as Labour Day, International Workers_ Day, or May Day. It is a celebration of the social and economic achievements of the labour movement. It originated from the eight-hour day movement, which advocated eight hours for work, eight for recreation, and eight for rest.
Prompt:	What are the main ingredients in pho, Vietnam_s iconic noodle soup?
FP16:	Rice noodles, beef or chicken, onions, ginger, cilantro, bean sprouts, basil, lime, hoisin sauce, Sriracha, and fish sauce.
MBOK:	Bone broth, rice noodles, fish sauce, herbs and spices, and beef, chicken, or seafood, depending on the type of pho you_re eating. Pho is usually served with bean sprouts, Thai basil, lime wedges, and hoisin and sriracha sauces.

G.6 Additional Baselines

G.6.1 Comparions with QuIP and ShiftAddLLM

Both QuIP (Chee et al., 2023) and ShiftAddLLM (You et al., 2024) are PTQ method for LLMs. QuIP is a two-step process that leverages the insight that quantization performs better when weight and Hessian matrices are incoherent. It uses an adaptive rounding procedure to minimize a quadratic proxy objective, which measures the error between the original and quantized weights. Additionally, it applies pre- and post-processing steps using random orthogonal matrices to ensure the weight and Hessian matrices are incoherent. Conversely, our method does not employ either these complicated pre- and post-processing steps or costly Hessian matrices. Meanwhile, ShiftAddLLM is a post-training reparameterization process, which quantizes each weight matrix in the LLM into a set of binary matrices and group-wise scaling factors. he original multiplication between activations and weights is then reparameterized into: (1) bitwise shifts for the activations, using the power-of-two quantized scaling factors, and (2) additions of the results, guided by the binary weight matrices; this process can be implemented using look-up tables (LUTs) on GPUs.

Table 8 presents results on OPT models, with competitor results extracted from their respective original papers. Notably, ShiftAddLLM utilizes a more computationally expensive group quantization, whereas our method does not. Our results clearly demonstrate that our approach consistently and significantly outperforms these baselines, particularly in the 2-bit scenario.

Table 8: Comparisons with QuIP, ShiftAddLLM using OPT models.

BIT-WIDTH	METHOD	OPT-125M	OPT-350M	OPT-1.3B
2	QuIP (Chee et al., 2023)	34.22	25.19	16.21
	ShiftAddLLM (You et al., 2024)	31.29	24.24	21.53
	MBOK [Ours]	**29.10**	**23.12**	**15.03**
3	QuIP (Chee et al., 2023)	347.40	672.30	41.64
	ShiftAddLLM (You et al., 2024)	51.15	40.24	29.03
	MBOK [Our]	**28.60**	**24.54**	**16.13**

G.6.2 COMPARIONS WITH BITSTACK, DB-LLM AND AWQ

While BitStack (Wang et al., 2025) also decompose weights using SVD, its core method and goal fundamentally differ from our method. BitStack is a training-free method primarily aimed at saving storage for inference. In contrast, our method not only converts FP models into Boolean models but also includes further fine-tuning, with the goal of achieving low complexity in both training and inference. Furthermore, while BitStack packs the extracted binary matrix into GPU-supported data types to reduce inference memory, and its approach to loading residual blocks relies on their influence on perplexity, our approach to residual block management is distinct.

DB-LLM (Chen et al., 2024) is limited to a fixed decomposition into two binary matrices, whereas our MBOK method generalizes to an arbitrary number of Boolean kernels. In DB-LLM, the full-precision knowledge is preserved only through scaling factors and binary matrices derived implicitly via thresholding. There is no formal analysis proving the optimality of this formulation. In contrast, thanks to the SVID in our approach, each extracted kernel is accompanied by an optimal scaling vector and Boolean matrix. This allows us to only finetune the last kernel to calibrate the entire model. Like most existing binary LLMs, DB-LLM relies on full-precision latent weights during training and finetuning. Our method does not require this, as it directly operates in the Boolean domain. This distinction is particularly important in the LLM context, where training and finetuning can be computationally expensive.

Table 9 compares our method, MBOK (with 2 kernels), against BitStack, DB-LLM, and AWQ (Lin et al., 2024) on LLaMA2-7B. It is evident that our method consistently outperforms all baselines.

Table 9: Comparisons with AWQ, BitStack, DB-LLM using LLaMA2-7B with 2-bit setting.

METHOD	Wiki2 (↓)	ARc-e (↑)	ARC-c (↑)	PIQA (↑)	Hella. (↑)	WinoG. (↑)
AWQ (Lin et al., 2024)	1.8e5	26.3	26.7	50.9	26.5	49.3
BitStack (Wang et al., 2025)	29.93	32.3	25.6	62.4	42.8	53.6
DB-LLM (Chen et al., 2024)	7.23	**45.2**	33.5	73.1	61.9	61.7
MBOK [Ours]	**6.87**	44.8	**34.2**	**75.0**	**65.6**	**61.7**

G.7 Effects of Knowledge Distillation

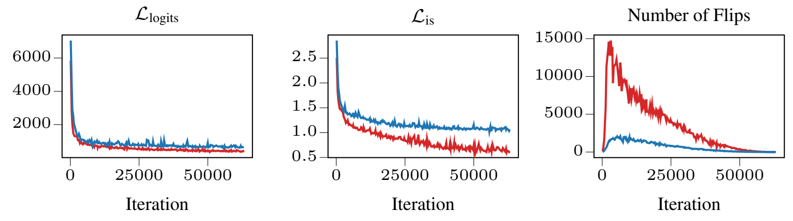

	Wiki2	C4
KD	**31.47**	**28.62**
No KD	32.21	29.84

Figure 13: Study on the effect of using knowledge distillation on OPT-125M with 2 Boolean kernels.

Fig. 13 presents a comparison between training with and without Knowledge Distillation (KD). It is evident that employing KD outperforms the baseline in terms of test perplexity on the Wiki2 and C4 datasets, as it provides more informative guidance during training. To investigate this behavior further, we visualize the convergence of $\mathcal{L}_{\text{logits}}$ and $\mathcal{L}_{\text{is}}$. Aided by the informative guidance from the teacher, convergence with KD is significantly faster. Furthermore, the model learns more effectively—leveraging the additional signal from the teacher—as evidenced by the higher flipping rates compared to training without KD.

G.8 Analysis of Scaling Values

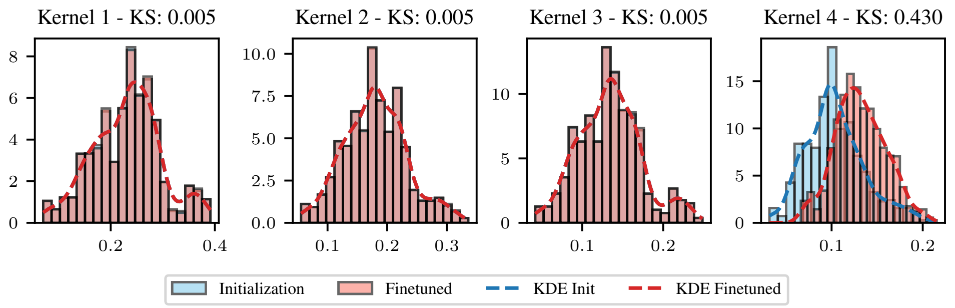

Figure 14: Histogram of output-scaling values for the first linear layer of OPT-125M with four kernels, shown at initialization and after finetuning. The Kolmogorov–Smirnov (KS) statistic is also reported to quantify the difference between the scaling-value distributions before and after finetuning.

Fig. 14 illustrates how the output-scaling values of the four kernels in the first linear layer change from initialization to after finetuning. All output-scaling values are learnable; however, only those associated with the last kernel exhibit a substantial shift during training. This is evident from both the histogram changes and the corresponding Kolmogorov–Smirnov distance.

After finetuning, the scaling values of the last kernel become significantly larger and more dominant, whereas the scaling values of the other kernels change only minimally. This observation supports our theoretical analysis: successive SVID extraction provides sufficiently strong initialization for the low-order kernels, and finetuning primarily the last kernel is already adequate.

G.9 Convergences of OPT Models

Fig. 15 shows the training convergences of MBOK using 3 kernels with OPT models.

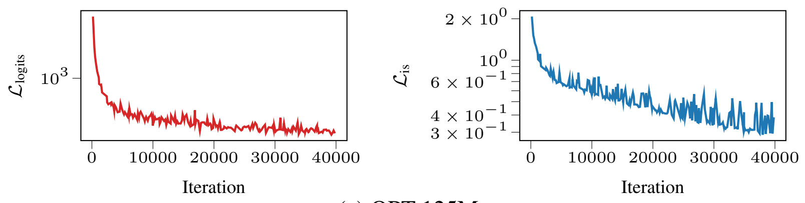

(a) OPT-125M

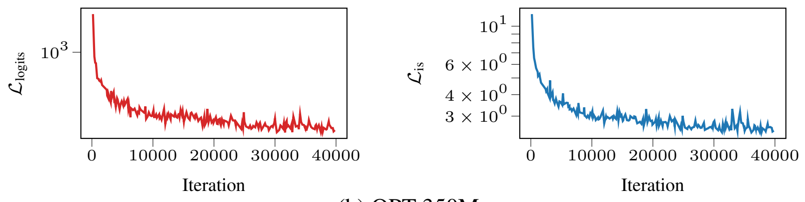

(b) OPT-350M

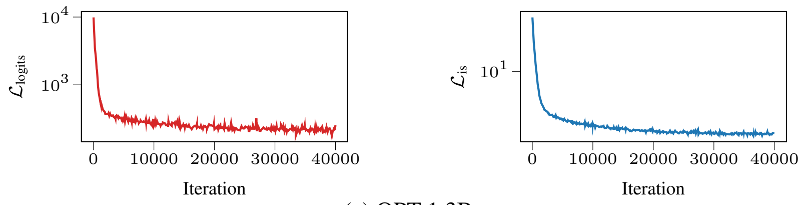

(c) OPT-1.3B

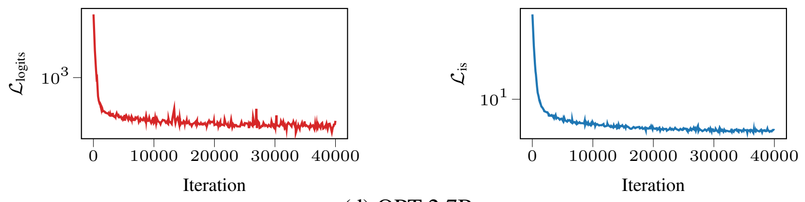

(d) OPT-2.7B

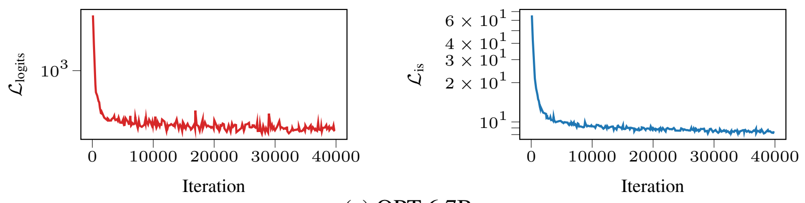

(e) OPT-6.7B

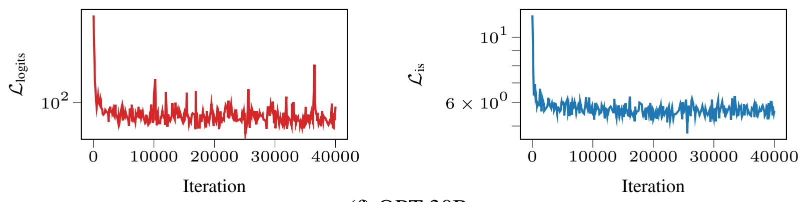

(f) OPT-30B

Figure 15: The training convergences of MBOK using 3 kernels with OPT models.

G.10 Effects of Successive SVID Initialization

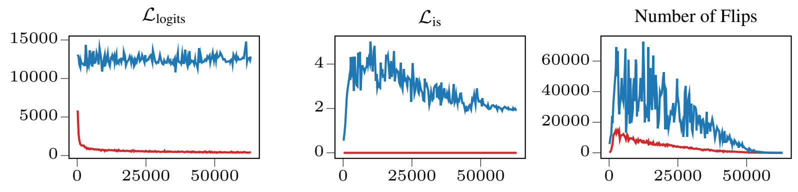

	Wiki2	C4
Suc. SVID	**31.47**	**28.62**
Rand. Init.	1.6E4	1.1E4

Figure 16: Study on the effect of using our successive SVID strategy and random initialization on OPT-125M with 2 Boolean kernels.

Fig. 16 compares our proposed successive SVID initialization with a random initialization. It is clear that our method delivers far better results, while the random initialization often fails to converge. Moreover, our initialization enables the model to learn efficiently, whereas the random initialization causes the model to struggle, as reflected by the large number of Boolean flips.

G.11 Discussion on Latency and Comparison with Vector Quantization

Scalar and Vector Quantization. In the context of LLMs, scalar quantization and vector quantization are two different approaches for compressing weights. Scalar quantization maps each weight or activation independently to a smaller set of discrete levels (e.g., 32-bit floating-point to 8- or 4-bit integers). It is simple, hardware-friendly, and widely used in practice, but it ignores correlations across dimensions, potentially discarding fine-grained structure. Vector quantization (VQ) instead compresses entire vectors (e.g., weight groups) by replacing them with indices into a learned codebook of representative vectors. By capturing cross-dimensional correlations, VQ often achieves higher compression, particularly for large embedding tables. However, codebook training is more complex, and inference requires index lookups to reconstruct vectors. This adds significant overhead to both quantization and dequantization, leading to much higher latency compared to scalar methods.

Our method is native 1-bit weight design, its nearest baselines are scalar weight quantization. As a result, for a fair comparison, in the main text we mainly consider state-of-the-art scalar quantization like OmniQuant (Shao et al., 2024), OPTQ (Frantar et al., 2023), LLM-QAT (Liu et al., 2024c) as the main baselines. Nevertheless, for completeness, we also compare our approach against state-of-the-art ultra low-bit vector quantization (VQ) methods for LLMs, including QTIP (Tseng et al., 2024b) and QUIP# (Tseng et al., 2024a) in a 2-bit setting, specifically on LLaMA-7B with a sequence length of 2048 (results taken from the QTIP paper). The results are summarized in Table 10. Remarkably, our method's performance is comparable to these state-of-the-art (SOTA) VQ methods. This is noteworthy given that our approach directly utilizes native Boolean weights, eliminating the need for the very costly quantization and dequantization of high-dimensional vectors inherent in VQ.

Table 10: Perplexity comparison with SOTA vector quantization methods using LLaMA-7B.

METHOD	Wiki2 (↓)	C4 (↓)
QUIP# (Tseng et al., 2024a)	6.86	8.36
QTIP (Tseng et al., 2024b)	6.52	7.99
MBOK [Ours]	6.83	8.53

Empirical Evidence of Latency Gains. To demonstrate the practicality of our approach even on modern hardware such as GPUs, we leverage the recently introduced BitBLAS library [1] (Wang et al., 2024) for 1-bit matrix multiplications. Using FP16 activations with INT1 weights, we measure the latency of linear layers in LLaMA-7B (Table 11) and LLaMA-13B (Table 12) under an inference batch size of 1, evaluating our method MBOK with two kernels. Our results show that MBOK achieves up to

[1] `https://github.com/microsoft/BitBLAS`

an 8.7× speedup over FP16 baselines, while substantially outperforming existing binarization and scalar quantization methods, as detailed in the main text. We also benchmark against 2-bit QUIP# and QTIP using the authors' official implementations[2][3]. All experiments are conducted on a Google Cloud A100 GPU.

Remarkably, our method is not only much faster than these VQ baselines but also delivers comparable performance. This is expected, as VQ-based methods incur significant overhead from the costly encoding and decoding steps required to realize their high compression ratios. Taken together, the results highlight that our native Boolean approach offers a compelling and efficient alternative to state-of-the-art vector quantization methods. With dedicated Boolean hardware accelerators, the performance gains would be even more pronounced.

Table 11: Measured latency (ms) of linear layers in LLaMA-7B, with values in parentheses denoting speed-up relative to the FP16 baseline.

WEIGHT SIZE	FP16	QUIP# (Tseng et al., 2024a)	QTIP (Tseng et al., 2024b)	MBOK (Ours)
4096×4096	0.10697	0.46196 (0.23×)	1.37137 (0.08×)	**0.04989 (2.14×)**
4096×11008	0.27935	0.55526 (0.50×)	3.13633 (0.09×)	**0.05136 (5.44×)**
11008×4096	0.27664	0.55988 (0.49×)	3.16067 (0.09×)	**0.05117 (5.41×)**

Table 12: Measured latency (ms) of linear layers in LLaMA-13B, with values in parentheses denoting speed-up relative to the FP16 baseline.

WEIGHT SIZE	FP16	QUIP# (Tseng et al., 2024a)	QTIP (Tseng et al., 2024b)	MBOK (Ours)
5120×5120	0.16540	0.62260 (0.27×)	1.96368 (0.08×)	**0.05074 (3.25×)**
5120×13824	0.42830	0.62836 (0.68×)	5.23681 (0.09×)	**0.05098 (8.40×)**
13824×5120	0.43411	0.62840 (0.69×)	5.21193 (0.08×)	**0.04987 (8.70×)**

H Ethics Statement

This work makes a fundamental contribution to machine learning methodology. It does not involve human subjects, sensitive data, or applications with direct societal or ethical risks. We do not foresee any immediate ethical concerns arising from this research.

I Reproducibility Statement

We provide detailed descriptions of all algorithms and illustrative code for the core components. Experiments are conducted on standard benchmarks using established testing procedures, and all experimental details and settings are fully declared to facilitate independent reproduction of our results.

J The Use of Large Language Models

We used large language models (LLMs) solely for non-substantive assistance, including grammar refinement and summarizing relevant literature. All research ideas, analyses, and conclusions are the authors' own.

[2]https://github.com/Cornell-RelaxML/quip-sharp
[3]https://github.com/Cornell-RelaxML/qtip